nature structural & molecular biology

STAT2 is an essential adaptor in USP18-mediated suppression of type I interferon signaling

Kei-ichiro Arimoto[1,8], Sara Löchte[2,8], Samuel A Stoner[1], Christoph Burkart[1], Yue Zhang[3], Sayuri Miyauchi[1], Stephan Wilmes[2], Jun-Bao Fan[1], Jürgen J Heinisch[2], Zhi Li[4], Ming Yan[1], Sandra Pellegrini[4], Frédéric Colland[5,7], Jacob Piehler[2] & Dong-Er Zhang[1,3,6]

Type I interferons (IFNs) are multifunctional cytokines that regulate immune responses and cellular functions but also can have detrimental effects on human health. A tight regulatory network therefore controls IFN signaling, which in turn may interfere with medical interventions. The JAK–STAT signaling pathway transmits the IFN extracellular signal to the nucleus, thus resulting in alterations in gene expression. STAT2 is a well-known essential and specific positive effector of type I IFN signaling. Here, we report that STAT2 is also a previously unrecognized, crucial component of the USP18-mediated negative-feedback control in both human and mouse cells. We found that STAT2 recruits USP18 to the type I IFN receptor subunit IFNAR2 via its constitutive membrane-distal STAT2-binding site. This mechanistic coupling of effector and negative-feedback functions of STAT2 may provide novel strategies for treatment of IFN-signaling-related human diseases.

Type I interferon (IFN) signaling has emerged as a highly complex regulatory network coordinating the host's defense against pathogens and cancer via expression of over 300 IFN-stimulated genes (ISGs)[1,2]. Proteins encoded by ISGs include cytokines and chemokines that modulate innate and adaptive immune responses, enzymes that specifically block growth and survival of pathogens, and transcription factors and other regulators that affect cell proliferation and survival. Many studies from human genetic diseases and mouse models have demonstrated that IFNs are essential for immune responses against infections and cancer development[3,4]. Therefore, IFNs have successfully been used to treat viral infections, autoimmune disorders, and cancer[5]. Most recently, it has been revealed that autonomous IFN responses in cancer cells are required for successful anticancer therapies, including conventional chemotherapies, targeted anticancer treatment, radiotherapy, and immunotherapy[4,6]. However, it is also known that high-dose IFN therapies cause severe acute and chronic side effects[7,8]. Furthermore, excess IFN production or dysregulated IFN signaling contributes to pathogenesis in people with systemic lupus erythematosus, Sjogren's syndrome, systemic sclerosis, rheumatoid arthritis, and the rare genetic disorders known as interferonopathies[9,10]. Together, these findings indicate that accurate fine-tuning of the IFN system is crucial for human health and for therapeutic interventions.

The binding of type I IFNs to the receptor subunits IFNAR1 and IFNAR2 induces the activation of their associated Janus family tyrosine kinases, TYK2 and JAK1, respectively[11]. Activated TYK2 and JAK1 in turn phosphorylate IFNAR2-associated STAT2 and STAT1, thereby resulting in formation of the DNA-binding STAT1–STAT2–IRF9 ternary complex IFN-stimulated gene factor 3 (ISGF3). ISGF3 promotes expression of genes with an IFN-stimulated response element in their promoters[12,13]. Signaling patterns elicited by type I IFNs strongly depend on the cellular and physiological context[14]. An intricate interplay of receptor dimerization dynamics and spatiotemporal modulation of IFN signaling by multiple positive and negative intracellular regulators[1,15] and by endocytosis[16] are likely to contribute to signaling plasticity[17]. Among these regulators, the ubiquitin-specific protease USP18, which we have previously identified in an analysis of gene expression in a leukemia-fusion-protein mouse model[18,19], plays an intriguing role. USP18 is an enzyme that removes a ubiquitin-like modifier, ISG15, from conjugated proteins[20]. However, USP18 expression is strongly stimulated by IFN treatment and exerts negative regulation of type I interferon signaling, an effect independent of its enzymatic activity[21]. By competing with JAK1 for binding IFNAR2, USP18 may interfere with the cytosolic stabilization of signaling complexes, because this stabilization is probably mediated by the Janus kinases. USP18 thereby decreases ligand binding, receptor dimerization and downstream signaling in a complex IFN-affinity-dependent manner[21–23]. Interestingly, in human cells, ISG15 directly regulates USP18 stability[24]. Furthermore, critical functions of USP18 in IFN-mediated immune responses have been demonstrated in mouse and human models[25–32], thus suggesting that USP18 has a broad effect on immune responses and that modulating USP18-inhibitory effects may have therapeutic potential.

[1]Moores UCSD Cancer Center, University of California San Diego, La Jolla, California, USA. [2]Department of Biology, University of Osnabrück, Osnabrück, Germany. [3]Division of Biological Sciences, University of California San Diego, La Jolla, California, USA. [4]Institut Pasteur, Cytokine Signaling Unit, Inserm, Paris, France. [5]Hybrigenics, impasse Reille, Paris, France. [6]Department of Pathology, University of California San Diego, La Jolla, California, USA. [7]Present address: Institut de Recherche Servier, Croissy-sur-Seine, France. [8]These authors contributed equally to this work. Correspondence should be addressed to J.P. (piehler@uos.de) or D.-E.Z. (d7zhang@ucsd.edu).

Received 8 August 2016; accepted 13 January 2017; published online 6 February 2017; doi:10.1038/nsmb.3378

While quantifying effector interactions with IFNAR2 in live-cell protein micropatterning assays, we have recently observed that recruitment of STAT2 is affected by USP18 (ref. 33), thus suggesting a functional cross-talk between these proteins. Among the seven mammalian STAT proteins, which are activated by diverse cytokines[34], STAT2 is unique in its selective involvement in type I and type III IFN signaling. Here, we investigated in detail the role of STAT2 in IFNAR desensitization by USP18, through use of live-cell micropatterning in real-time protein interaction assays and single-molecule imaging in combination with protein biochemical approaches. We found that, beyond being a key effector of IFN signaling, STAT2 is essential for the USP18-mediated inhibition of JAK–STAT signaling. STAT2 directly interacts with USP18 and thus mediates its recruitment to IFNAR2. In turn, anchored USP18 interferes with receptor dimerization and JAK phosphorylation. Elucidating this previously unrecognized requirement of STAT2 in negative-feedback regulation should expand the potential for local or systemic modulation of IFN signaling in treating human disease.

RESULTS

USP18 interacts with STAT2

The role of USP18 in IFN signaling is independent of its ISG15-deconjugating activity but relies on its interaction with IFNAR2 (refs. 21,35). To identify proteins that may regulate USP18 function in the IFN signaling pathway, we conducted a yeast two-hybrid screen by using wild-type human full-length USP18 and its active site mutant (C64A) as bait proteins. We identified 11 independent clones encoding STAT2. Likewise, direct interaction of STAT2 and USP18 was detected in a targeted yeast two-hybrid assay (**Fig. 1a**). Coimmunoprecipitation showed interaction between exogenously expressed USP18 and STAT2 (**Fig. 1b**). Furthermore, a pulldown analysis revealed direct binding between biochemically purified STAT2 and USP18 (**Fig. 1c**).

To quantify the interaction between STAT2 and USP18 in live cells, a cell micropatterning approach for spatially controlled immobilization of bait proteins in the plasma membrane via the HaloTag[33] was used (**Supplementary Fig. 1a**). This technique quantifies equilibrium binding to a target protein within the cell *in situ* and thus nicely complements coimmunoprecipitation data with respect to functional relevance. Colocalization of STAT2 and USP18 together with micropatterned IFNAR2 confirmed that both STAT2 and USP18 constitutively interacted with IFNAR2 (**Supplementary Fig. 1b–d**). Interaction dynamics was analyzed by fluorescence recovery after photobleaching (FRAP) and revealed similar rate constants for STAT2 (τ_{STAT2} of 79 ± 28 s, mean ± error of fit) and USP18 (τ_{USP18} of 103 ± 33 s; **Supplementary Fig. 1e**), thus suggesting simultaneous interaction of both proteins with IFNAR2. We next used cell micropatterning to examine the IFNAR2-independent interaction of STAT2 and USP18 in IFNAR2-deficient U5A cells. A fusion protein of STAT2 with a transmembrane domain (TMD) as well as extracellular mTagBFP and HaloTag (HaloTag-mTagBFP-TMD-STAT2) was used as bait (**Fig. 1d**). Coexpression of this construct with mEGFP-tagged USP18 revealed strong colocalization within micropatterns, as quantified by the contrast between the patterned and nonpatterned regions in the cells. No significant contrast was observed when only mEGFP was coexpressed with STAT2 as bait or when USP18 was cotransfected with a transmembrane domain that was not fused to STAT2 (**Fig. 1d**; box plot). Monitoring of the exchange kinetics of intracellular USP18 bound to micropatterned STAT2 by FRAP (**Fig. 1d**) yielded a mean interaction lifetime of $\tau = 53 \pm 28$ s (8 cells analyzed). Furthermore, using 2fTGH, MDA-MB-231, and KT-1 cells, we confirmed the interaction of endogenous USP18 and STAT2 through coimmunoprecipitation assays (**Fig. 1e**). Together, these different approaches clearly established that STAT2 directly binds USP18.

STAT2 is required for inhibition of type I IFN signaling by USP18

To examine the role of STAT2 in USP18-mediated desensitization of type I IFN signaling, we used the following U-series cell lines derived from human fibrosarcoma 2fTGH cells: U1A (*TYK2*$^{-/-}$), U2A (*IRF9*$^{-/-}$), U4A (*JAK1*$^{-/-}$), U5A (*IFNAR2*$^{-/-}$), and U6A (*STAT2*$^{-/-}$)[36,37]. These cells were stably transduced with the MIP control or MIP-USP18 (**Fig. 2a–e**). As expected, in cells lacking TYK2 (U1A), JAK1 (U4A), and IFNAR2 (U5A), phosphorylation of STAT1 was not observed after IFNα treatment (**Fig. 2b**,**d**,**e**), because important components of the signaling pathway were missing. In 2fTGH and U2A cells, USP18 expression clearly decreased STAT1 phosphorylation after IFNα treatment (**Fig. 2a**,**c**), thus indicating that USP18 inhibits IFN signaling upstream of IRF9, as reported previously[21]. Interestingly, expression of USP18 did not affect STAT1 phosphorylation in STAT2-deficient U6A cells (**Fig. 2f**), thus suggesting that STAT2 is required for USP18-mediated inhibition. Notably, IFN-induced STAT1 phosphorylation was much weaker in U6A cells than in 2fTGH cells (**Fig. 2g**), because STAT2 supports STAT1 phosphorylation[38]. To further verify the critical role of STAT2, we used mouse embryonic fibroblasts (MEFs) derived from *Stat2*-knockout mice (*Stat2*$^{-/-}$). In these cells, ectopic Usp18 did not inhibit IFNβ-induced STAT1 phosphorylation (**Fig. 2h**, lanes 1–4). STAT2 transduction strongly increased IFNβ-stimulated STAT1 phosphorylation, but in this context ectopic USP18 had a strong inhibitory effect (**Fig. 2h**, lanes 5–8). These results indicate that, in addition to physically interacting with USP18, STAT2 plays a critical role in mediating the negative effect of USP18 on type I IFN signaling.

To investigate whether the inhibitory effect of STAT2 plus USP18 could be detected upstream of STAT1 phosphorylation, we examined JAK1 phosphorylation. Exogenously expressed USP18 did not affect JAK1 phosphorylation in *Stat2*$^{-/-}$ MEFs but clearly diminished JAK1 phosphorylation in Stat2-transduced *Stat2*$^{-/-}$ MEFs (**Fig. 2i**), thereby indicating that STAT2 is critical for USP18-mediated inhibition of JAK1 phosphorylation. To confirm this finding, we also selected an effective Stat2 short hairpin RNA (shRNA) to knock down Stat2 expression (**Fig. 2j**). Neither control shRNA nor Stat2-specific shRNA affected IFNβ-induced JAK1 phosphorylation in *Usp18*$^{-/-}$ primary mouse bone-marrow cells (**Fig. 2k**). In contrast, expression of a Stat2 shRNA, but not a control shRNA, abolished the negative effect of exogenously expressed USP18 on JAK1 phosphorylation. These results further support that STAT2 is required for USP18-mediated inhibition, which occurs upstream of STAT phosphorylation.

To further examine the mechanistic requirement for STAT2 in USP18-dependent negative regulation of IFN signaling, we examined the expression of 23 IFN-inducible genes in *Stat2*$^{-/-}$ MEFs transduced with control or Usp18 expression vectors, with or without exogenous reintroduction of Stat2. As expected, the majority of genes tested (21 of 23) were not induced by IFN treatment in the absence of STAT2 (representative genes shown in **Supplementary Fig. 2a**). We did, however, identify two genes (*Irf9* and *Cxcl9*) that showed weak induction of expression in the absence of STAT2 (**Supplementary Fig. 2b**). Importantly, USP18-mediated inhibition of expression of these ISGs was observed only after reintroduction of STAT2 (**Supplementary Fig. 2a**,**b**). These observations fully support the essential biological role of STAT2 in IFN-responsive signal transduction[39]. Furthermore, both of our biochemical and gene-expression analyses demonstrate the mechanistic requirement for STAT2 in USP18-mediated inhibition of interferon signaling.

STAT2 coiled-coil and DNA-binding domains and inhibition of IFN signaling by USP18

Structurally, STAT2 can be divided into N-terminal (NTD), coiled-coil (CC), DNA-binding (DB), linker (LD), Src homology 2 (SH2) dimerization, and C-terminal transactivation domains (**Fig. 3a**). In this study, we included the LD in the DB, because the LD is required for the appropriate DB structure[40]. To understand the mechanism of STAT2 in USP18-mediated inhibition of IFN signaling for potential therapeutic applications, we performed coimmunoprecipitation assays on a set of STAT2-deletion mutants (**Fig. 3a**). FLAG-tagged

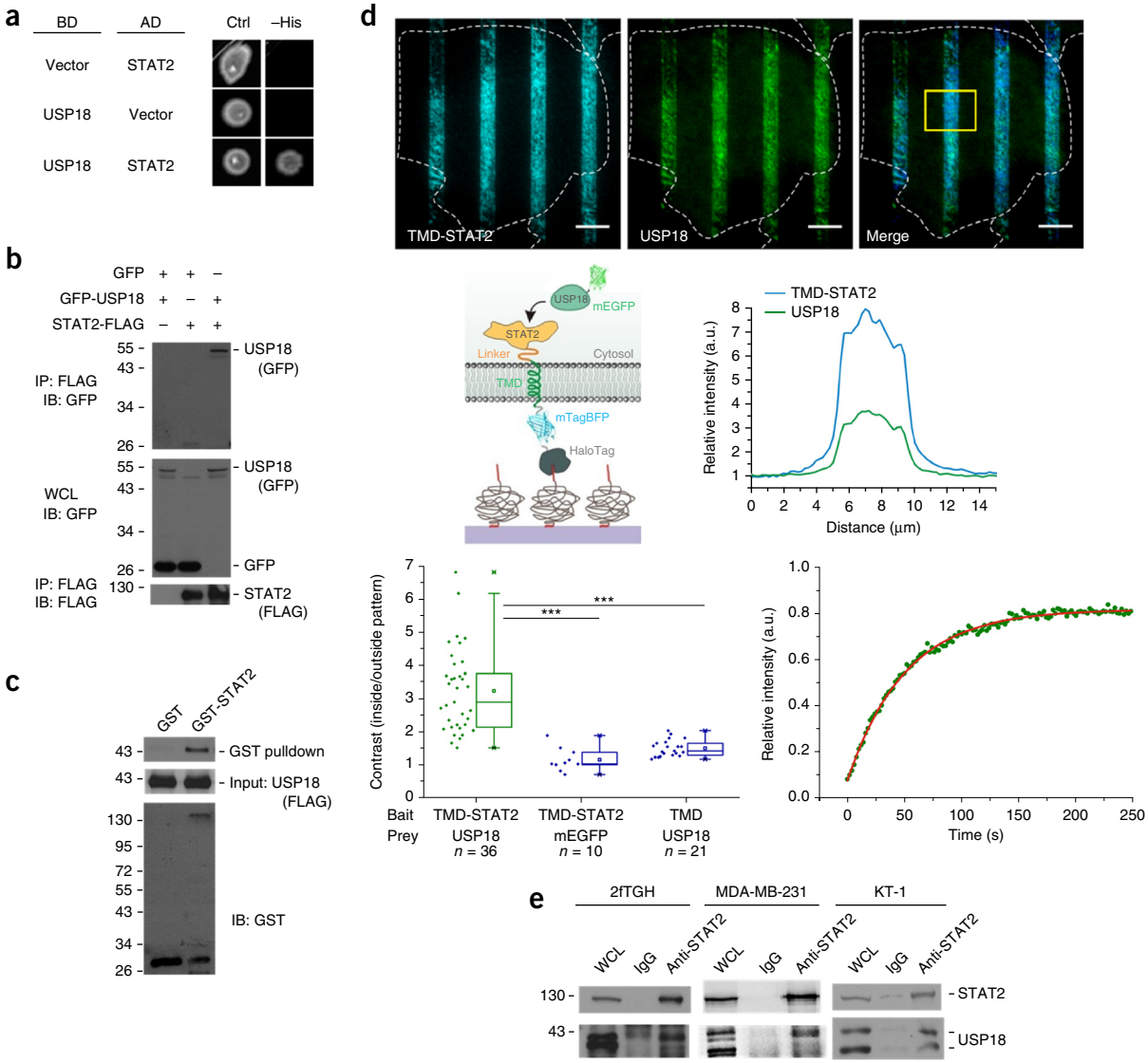

Figure 1 USP18 interacts with STAT2. (**a**) Yeast two-hybrid analysis of the direct interaction between USP18 and STAT2. Overnight cultures of strains pJ69-4a/pJ69-4α carrying two-hybrid plasmids were spotted onto selective medium (control (ctrl), –leucine, –tryptophan, for plasmid maintenance and growth control; –histidine, in addition to –leucine, –tryptophan, to select for interaction). BD, DNA-binding-domain fusion; AD, activation-domain fusion. (**b**) Immunoblot (IB) analysis of whole cell lysates (WCL) and anti-FLAG immunoprecipitates (IP) derived from 293T cells 24 h after cotransfection with plasmids encoding GFP, GFP-USP18, and STAT2-FLAG. Numbers on the left show molecular weight (kDa). (**c**) GST pulldown assay showing that the STAT2 directly associates with USP18. Numbers on the left show molecular weight (kDa). (**d**) Immobilization of STAT2 to probe for direct interaction with USP18. Top left, cartoon schematic of experimental setup. U5A cells were transfected with mEGFP-USP18 and with the STAT2 intracellular region fused to a transmembrane domain (TMD) and extracellular mTagBFP and HaloTag. Top middle, representative images of a transfected cell (out of 36 cells analyzed) whose outline is shown with dashed lines, in the blue channel (TMD-STAT2) and green channel (USP18); scale bars, 10 μm. Top right, graph showing normalized (norm.) intensity profiles of both channels within the yellow region of interest depicted in the merged image. A.u., arbitrary units. Bottom left, quantitative analysis of the recruitment of mEGFP-USP18 to micropatterned STAT2, as determined on the basis of the contrast of the fluorescence intensities inside and outside the patterns. As negative controls (blue boxes), U5A cells were transfected with mEGFP-USP18 and HaloTag-mTagBFP-TMD and with mEGFP and HaloTag-mTagBFP-TMD-STAT2. Box plots show median (line), mean (open squares), first and third quartiles (box limits) and 1.5× the interquartile range (whiskers). Points, individual cells for which measurements were performed; x, first and 99th percentiles. The number of cells analyzed (obtained from two independent experiments) is shown below each group. ***$P < 0.001$ by two-sample Kolmogorov–Smirnov test. Bottom right, fluorescence recovery of USP18 recruited to micropatterned STAT2, and monoexponential fit of the recovery curve (representative of 8 cells analyzed). (**e**) Immunoblot showing interaction of endogenous USP18 and STAT2 in 2fTGH, MDA-MB-231, and KT-1 cells. Lysates from cells treated with IFNα (1,000 U/ml) for 24 h were immunoprecipitated with IgG or anti-STAT2 and immunoblotted with anti-STAT2 or anti-USP18. Numbers on the left show molecular weight (kDa). Uncropped blot images are shown in **Supplementary Data Set 1**.

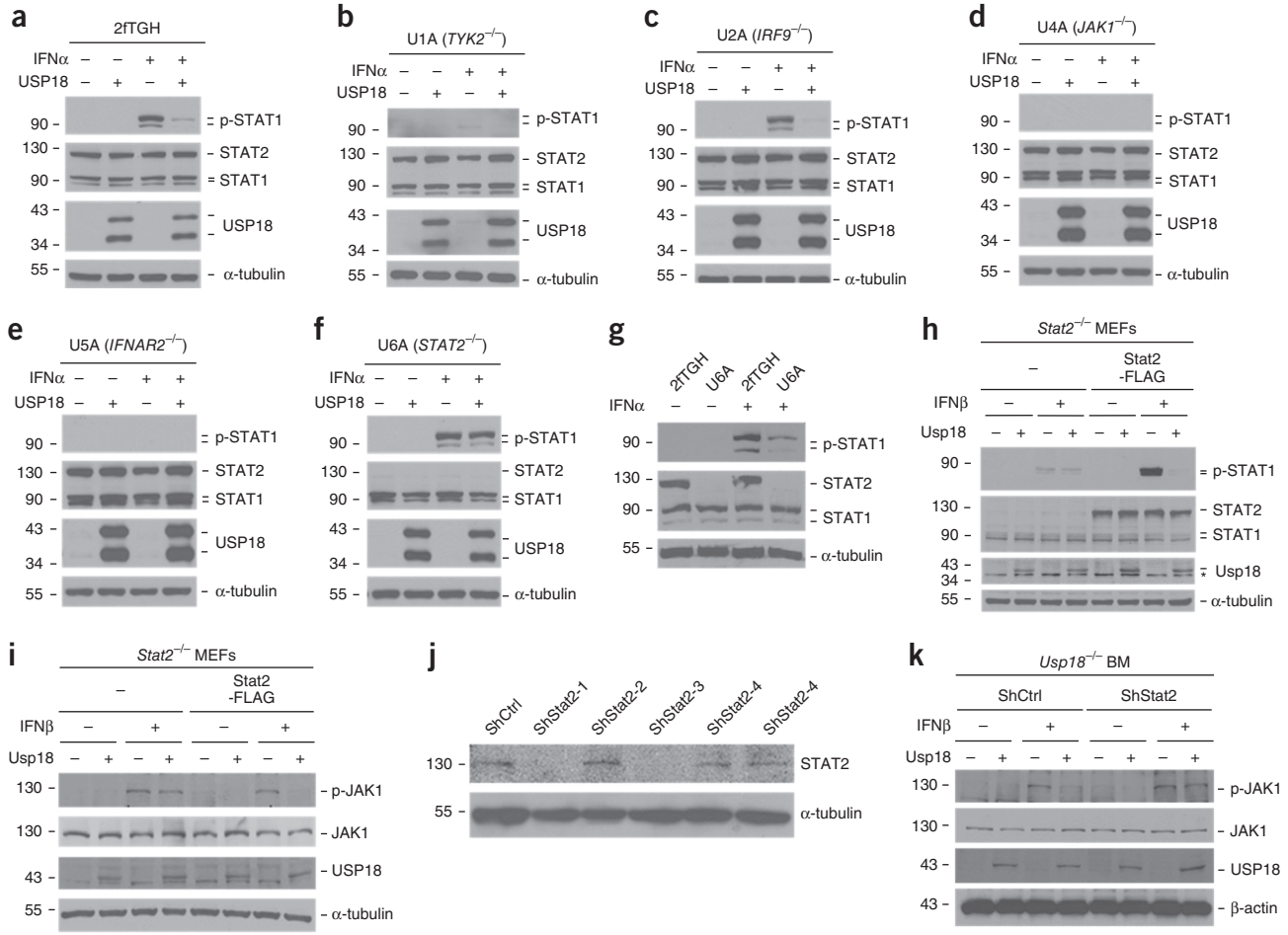

Figure 2 STAT2 is required for USP18-mediated inhibition of type I IFN signaling. Numbers on the left show molecular weight (kDa). (**a**–**f**) Immunoblots of different indicated cells expressing MIP or MIP-USP18, treated with IFNα (1,000 U/ml) for 15 min. The cell lysates were immunoblotted with the indicated antibodies. P-, phospho-. (**g**) Immunoblot analysis of STAT1 phosphorylation in 2fTGH and U6A cells in the presence or absence of (1,000 U/ml) IFNα. (**h**,**i**) Immunoblots from *Stat2*$^{-/-}$ MEFs infected with MIP control (–) or MIP-Usp18 (+) retroviruses, in either the presence or absence of rescue with C-terminally FLAG-tagged Stat2 cDNA. Cells were treated with either mouse IFNβ (500 U/ml) for 15 min (**h**) or 30 min (**i**), before cell lysates were collected and analyzed by immunoblotting with the indicated antibodies. (**j**) Immunoblot showing validation of Stat2 knockdown. Ba/F3 cells were infected with control (ShCtrl) or one of five Stat2-targeting shRNA (ShStat2) lentiviruses, after 5 d of puromycin selection. (**k**) Immunoblot of *Usp18*$^{-/-}$ bone-marrow (BM) cells infected with pCX4-bsr control (–) or pCX4-bsr-Usp18 (+), in either the presence or absence of control or Stat2 shRNA (ShStat2-3) expression. Two days after double drug selection (with puromycin and blasticidin), cells were either left untreated (–) or were treated (+) with mouse IFNβ (500 U/ml) for 30 min before cell lysates were collected and analyzed with the indicated antibodies. Uncropped images are shown in **Supplementary Data Set 1**.

USP18 (FLAG-USP18) was coexpressed with Myc-tagged STAT2 (STAT2-Myc) or either of three fragments of STAT2 (amino acids (aa) 1–136 of the NTD; aa 139–572, containing the CC and DB domains; and aa 573–861, containing the SH2 and transactivation domains). The NTD and the C-terminal region of STAT2 did not coprecipitate with USP18. However, the protein with only the CC and DB domains of STAT2 significantly interacted with USP18 (**Fig. 3b**). Furthermore, immunoprecipitation of either USP18 (**Fig. 3c**) or wild-type or deletion-mutant STAT2 (**Fig. 3d**) revealed that the CC-only-deleted or DB-only-deleted STAT2 were able to associate with USP18. However, deletion of both CC and DB domains of STAT2 led to a loss of coprecipitation with USP18. Thus, these analyses suggest that both the CC and DB domains of STAT2 contribute to its interaction with USP18.

To examine the role of the STAT2-USP18 interaction in negative-feedback regulation of IFN signaling, we expressed an empty-vector control, full length STAT2, or deletion mutants of STAT2 in U6A cells. USP18 expression decreased STAT1 phosphorylation in STAT2-expressing U6A cells (**Fig. 4a**). Furthermore, the negative effect of USP18 was detected in the presence of STAT2 lacking the CC domain (**Fig. 4b**) or the DB domain (**Fig. 4c**). In contrast, although STAT2 lacking both CC and DB domains still promoted IFNα-induced STAT1 phosphorylation, it did not support the inhibitory function of USP18 (**Fig. 4d**), thus suggesting that the interaction of these two proteins via the CC and DB domains of STAT2 is crucial for the effect of USP18 on IFN signaling. Importantly, expression of USP18 and different STAT2 constructs did not affect the cell-surface levels of the IFN-receptor subunits IFNAR1 and IFNAR2 in these cell lines (**Fig. 4e**).

The N- and C-terminal regions of USP18 bind STAT2 and IFNAR2

On the basis of our previous report[21] and the results presented above, USP18 interacts with both IFNAR2 and STAT2. We therefore assessed which regions of USP18 are required for its interaction with STAT2 and IFNAR2. We generated six constructs for expression of selected regions of USP18 (**Supplementary Figs. 3a** and **4a**). In coimmunoprecipitation assays conducted with cell lysates containing

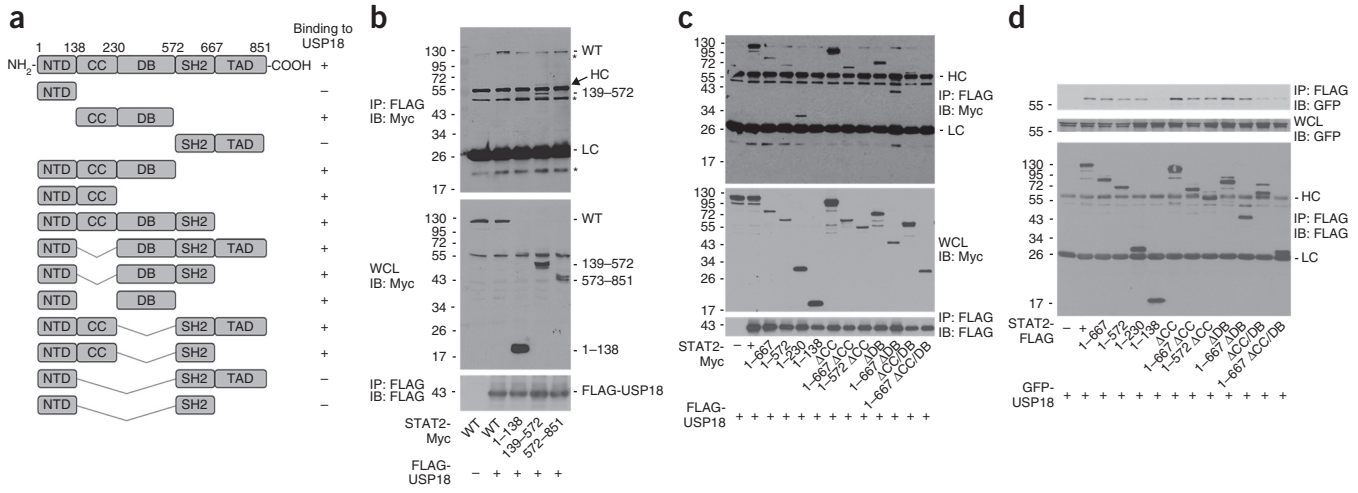

Figure 3 Both the coiled-coil (CC) and DNA-binding (DB) domains of STAT2 are involved in the interaction with USP18. (**a**) Schematic drawing of the STAT2 domain structure and deletion mutants used in this study. The ability of a given deletion mutant to interact with USP18 (+ or – binding) is indicated. (**b**,**c**) Immunoblot analysis of whole cell lysates (WCL) and anti-FLAG IP derived from 293T cells 24 h after cotransfection with plasmids encoding FLAG-USP18 and either the full-length STAT2-Myc (WT) or the indicated deletion mutants. (**d**) Immunoblot analysis of WCL and anti-FLAG IP derived from 293T cells 24 h after cotransfection with plasmids encoding GFP-USP18 and either STAT2-FLAG or the indicated deletion mutants. Asterisks indicate nonspecific bands. HC, heavy chain; LC, light chain. Numbers on the left in **b**–**d** show molecular weight (kDa).

FLAG-tagged USP18 and Myc-tagged STAT2, aa 1–112, aa 51–242, aa 1–242, and aa 243–312, but not aa 113–242 and aa 313–372 of USP18 interacted with STAT2, thereby suggesting that aa 51–112 and aa 243–312 of USP18 are two important regions for the STAT2-USP18 interaction (**Supplementary Fig. 3b**). Further analysis revealed that aa 303–312 of USP18 interacted with STAT2 (**Supplementary Fig. 3c**). Consequently, a mutant of USP18 with aa 303–312 deleted (USP18Δ303–312) was unable to suppress IFNα-induced STAT1 phosphorylation (**Supplementary Fig. 3d**).

We also established human KT-1 cell lines stably expressing wild-type USP18 or the noninteracting mutant USP18Δ303–312. After addition of IFNα, cells expressing wild-type USP18-showed a strong inhibition of phosphorylation of JAK1 and STAT1. USP18Δ303–312 did not show such a negative effect (**Supplementary Fig. 3e**), in agreement with its loss of STAT2 interaction.

Regarding the USP18-IFNAR2 interaction, peptides comprising aa 1–112, aa 1–242, and aa 313–372, but not aa 51–242, aa 113–242, and aa 243–312 of USP18 coimmunoprecipitated with the intracellular domain

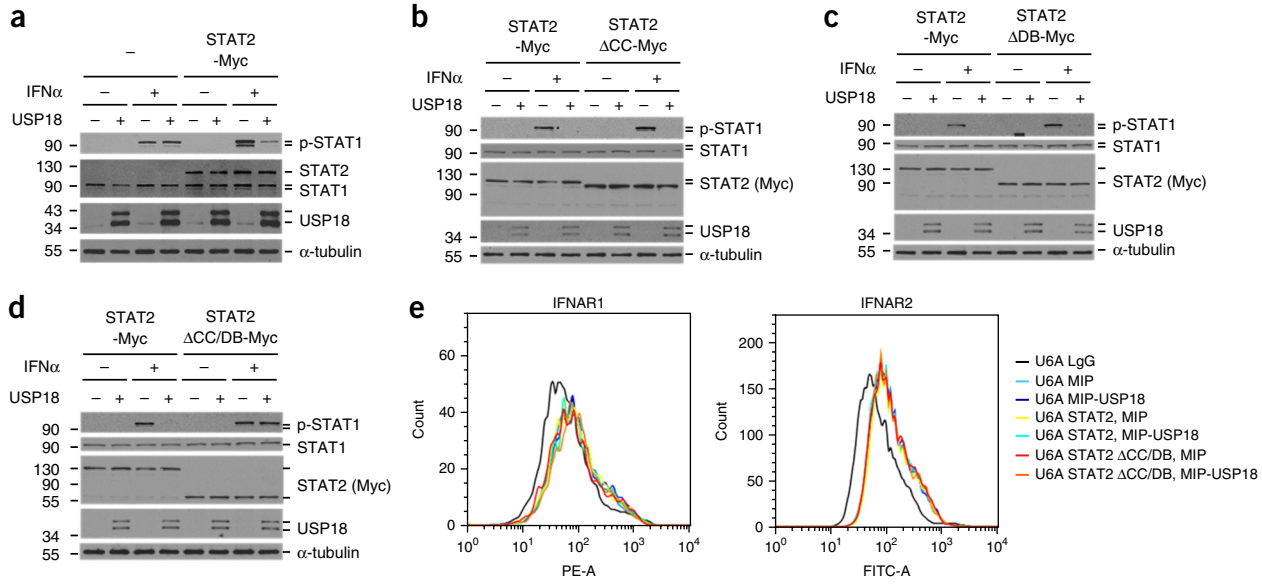

Figure 4 The coiled-coil (CC) and DNA binding (DB) domains of STAT2 are important for USP18-mediated inhibition of type I IFN signaling. (**a**) Immunoblot analyses of U6A cells stably transduced with control (–) or C-terminally Myc-tagged STAT2 (STAT2-Myc), infected with MIP control (–) or MIP-USP18 (+) retrovirus; with or without IFNα (1,000 U/ml) treatment for 15 min. Cell lysates were collected and analyzed with the indicated antibodies. (**b**–**d**) Immunoblot analysis of U6A cells stably transduced to express full-length STAT2 (STAT2-Myc) or STAT2-deletion mutants STAT2ΔCC-Myc (**b**), STAT2ΔDB-Myc (**c**), or STAT2ΔCC/DB-Myc (**d**), with or without IFNα (1,000 U/ml) treatment for 15 min. Cell lysates were collected and analyzed with the indicated antibodies. Numbers on the left show molecular weight (kDa). (**e**) Histograms showing the surface expression of IFNAR1 and IFNAR2 after infection of U6A cells with the indicated constructs.

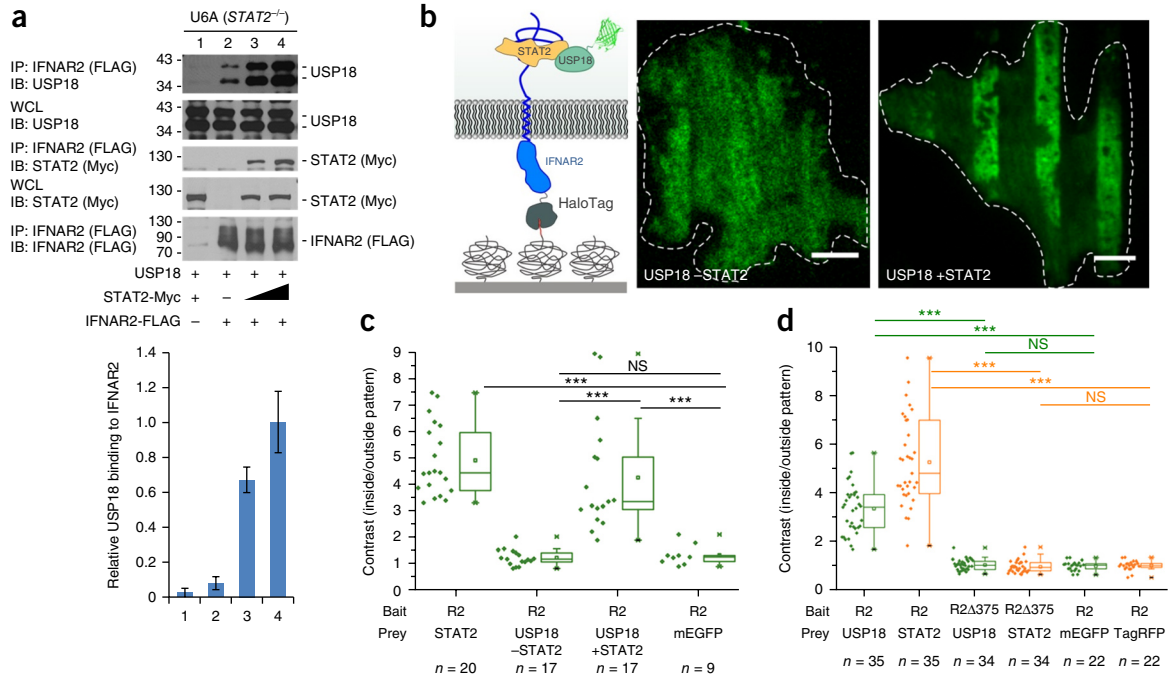

Figure 5 STAT2 recruits USP18 to IFNAR2. (**a**) Top, immunoblot analysis of whole cell lysates (WCL) and anti-FLAG IP derived from U6A cells 24 h after cotransfection with plasmids encoding USP18, FLAG-IFNAR2 and increasing amounts of STAT2-Myc expression construct. Numbers on the left show molecular weight (kDa). Bottom, quantification of the binding of USP18 to IFNAR2, shown as the ratio of IFNAR2-bound USP18 to total USP18, normalized to the maximum binding (lane 4). Bar graph shows mean and s.e.m. from 3 independent experiments. (**b**) Recruitment of USP18 and STAT2 to micropatterned IFNAR2 in STAT2-deficient U6A cells. Left, cartoon schematics of the experimental setup. Right, green-channel images of U6A cells transfected with HaloTag-mTagBFP-IFNAR2 and mEGFP-USP18 (USP18 –STAT2) or with HaloTag-mTagBFP-IFNAR2, mEGFP-USP18 and STAT2-TagRFP-T (USP18 +STAT2). Cell outlines are shown by dashed lines; each image is representative of 17 cells from two independent experiments. Scale bars, 10 μM. (**c**) Quantification of the recruitment of USP18 to immobilized IFNAR2 (R2) into micropatterns in U6A cells, on the basis of the contrast of the fluorescence intensities inside and outside the patterns. For comparison, constitutive binding of STAT2 (positive control) and cytosolic mEGFP (negative control) to micropatterned full length IFNAR2 expressed in U6A cells was quantified. (**d**) The C-terminal STAT2-interacting region of IFNAR2 is necessary for recruiting USP18. Quantification of recruitment of mEGFP-USP18 coexpressed with STAT2-TagRFP-T to immobilized HaloTag-IFNAR2 or C-terminally truncated HaloTag-IFNAR2 (R2375) in HeLa cells. As negative controls, HeLa cells were transfected with cytosolic mEGFP or TagRFP-T, respectively. In **c** and **d**, box plots show median (line), mean (open squares), first and third quartiles (box limits), and 1.5× the interquartile range (whiskers); outliers are plotted as individual points, and x denotes the first and 99th percentiles. Numbers of cells analyzed (from two independent experiments) are shown below each group. ***$P < 0.001$ by two-sample Kolmogorov–Smirnov test; NS, not significant.

(ICD) of IFNAR2 (**Supplementary Fig. 4b**). These results suggest that aa 1–51 and aa 313–372 of USP18 are important for the IFNAR2-USP18 interaction. Further analysis narrowed the first interaction domain to aa 36–51 of USP18 (**Supplementary Fig. 4c**,**d**). In line with this result, expression of aa 36–372, but not aa 51–372, of USP18 inhibited STAT1 phosphorylation after IFNα treatment (**Supplementary Fig. 4e**). Together, these findings indicate that aa 36–51 and aa 313–371 of USP18 are critical for the USP18-IFNAR2 interaction and that aa 51–112 and aa 303–312 of USP18 are important for the USP18-STAT2 interaction. We therefore conclude that the N- and C-terminal regions (aa 36–51 and aa 317–371) of USP18 play important roles in the interaction with IFNAR2, and the adjacent regions (aa 51–112 and aa 303–312) are critical for USP18 binding to STAT2.

STAT2 recruits USP18 to IFNAR2

These results established that USP18 independently interacts with IFNAR2 and STAT2. Because STAT2 itself constitutively interacts with IFNAR2 (refs. 33,41,42), we further examined whether interaction between USP18 and IFNAR2 was affected by STAT2. In STAT2-deficient U6A cells, the USP18-IFNAR2 interaction was enhanced up to ten-fold after expression of STAT2 (**Fig. 5a**). The importance of STAT2 in USP18 recruitment was also verified by live-cell micropatterning: whereas no binding of USP18 to micropatterned IFNAR2 was detectable in U6A cells, a strong increase in contrast after complementation with STAT2 was observed (**Fig. 5b**,**c**). In HeLa cells, the endogenous expression level of STAT2 was sufficient to yield substantial binding of USP18 bound to micropatterned IFNAR2 (**Supplementary Fig. 5c**). However, substantially increased USP18 binding was observed after ectopic coexpression of STAT2. These results highlight the critical role of STAT2 concentration in the effective recruitment of USP18 to IFNAR2. In the absence of STAT2, binding of USP18 was weakened, such that no significant recruitment of USP18 to micropatterned IFNAR2 was detectable in this experimental system. A comparable loss in USP18 binding to IFNAR2 was observed in the presence of STAT2 after deletion of the STAT2-binding site on IFNAR2, which has been suggested to include at least aa 418–444 (ref. 41). The recruitment of STAT2 and USP18 to IFNAR2 C-terminally truncated at position 375 was strongly decreased (**Fig. 5d** and **Supplementary Fig. 5c**). Mapping the STAT2 and USP18 binding to IFNAR2 by cell micropatterning of further deletions and mutations (**Supplementary Fig. 5d**–**f**) confirmed aa 418–444 of IFNAR2 as the minimal interaction site for STAT2 and USP18. These results established that the interaction of USP18 and STAT2 is responsible for recruitment of USP18 to IFNAR2 and is critical for the negative effect

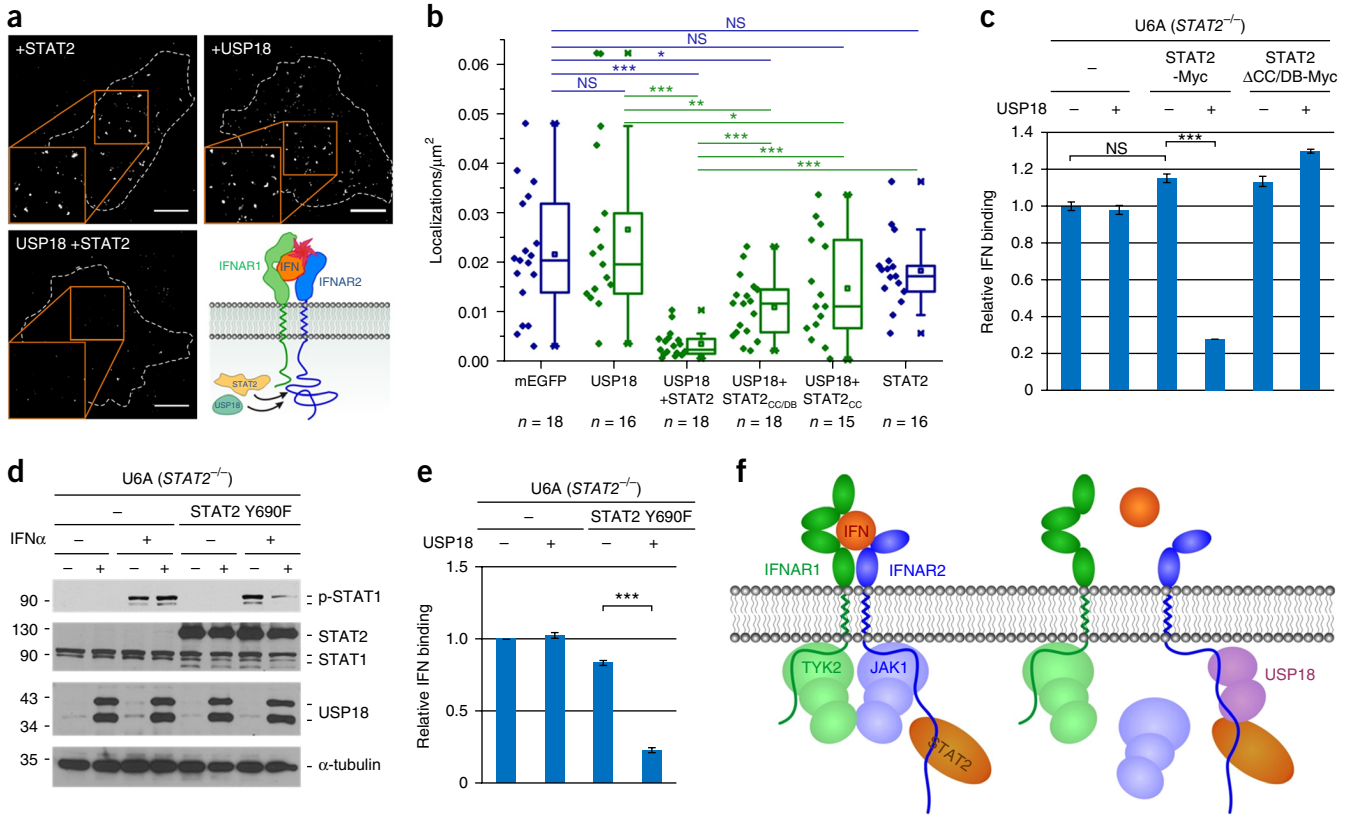

Figure 6 STAT2-USP18 interaction regulates ternary-complex assembly of the type I IFN receptor. (**a**) Binding of ^{DY647}IFNα2 M148A to the IFNAR at the surface of U6A cells expressing STAT2-TagRFP-T (top left), USP18-mEGFP (top right), or both (bottom left). The images are superimpositions of single-molecule localizations from 100 consecutive frames. Scale bars, 10 μm. Images are representative of 13–18 cells analyzed for each condition. (**b**) Comparison of the density of ^{DY647}IFNα2 M148A bound to cell-surface IFNAR in U6A cells expressing STAT2, USP18, or both proteins. Constructs corresponding to the STAT2 CC domain or CC and DB domains were also used in the assay. As a control, localization of ^{DY647}IFNα2 M148A on the surface of U6A cells transfected with mEGFP was quantified. Box plots show median (line), mean (open squares), first and third quartiles (box limits), and 1.5× the interquartile range (whiskers); outliers are plotted as individual points, and x denotes the first and 99th percentiles. The numbers of cells analyzed for each condition (from 2 independent experiments) are shown below each group. ***$P < 0.001$; **$P < 0.01$; *$P < 0.05$; NS, not significant by two-sample Kolmogorov–Smirnov test. (**c**) Relative amount of FITC-labeled IFNα bound to the U6A cell surface, as examined by flow cytometry. Cells were transduced to express the indicated constructs. Data are normalized to the mean fluorescence intensity (MFI) of U6A cells in the absence of STAT2 and USP18. Graph shows means and s.e.m. from 3 independent experiments. (**d**) Immunoblot analysis of U6A cells stably transduced with control (–) or C-terminally Myc-tagged STAT2 Y690F mutant (STAT2 Y690F) and infected with MIP (–) or MIP-USP18 (+) retrovirus, with or without IFNα (1,000 U/ml) treatment for 15 min. Cell lysates were analyzed with the indicated antibodies. Numbers on the left show molecular weight (kDa). (**e**) Relative amounts of FITC-labeled IFNα bound to the U6A cell surface, as examined by flow cytometry. Data are normalized to the MFI of U6A cells in the absence of STAT2 and USP18. Graph shows mean and s.e.m. from 3 independent experiments. ***$P < 0.001$., NS, not significant by two-tailed Student's *t*-test. (**f**) Model of USP18-STAT2 regulation of the IFN response.

of USP18 on type I IFN–induced JAK1 phosphorylation (**Fig. 2i–k**), which is upstream of type I IFN–induced STAT1 activation.

STAT2-USP18 interaction regulates assembly of the type I IFN receptor

We have recently reported that human USP18 negatively regulates the binding affinity of type I IFNs to their cell-surface receptor, thus decreasing the responsiveness of IFN-primed cells to subsequent IFN stimulation[22,23]. Quantitative single-molecule dimerization assays have revealed that USP18 interferes with the assembly of the ternary IFN–IFNAR1–IFNAR2 complex, thereby explaining the loss in ligand binding affinity[22]. To explore whether the STAT2-USP18 interaction is important for the effect of USP18 on ligand binding and ternary-complex formation, ligand binding assays in U6A cells were performed. To this end, we quantified the binding of IFNα2 M148A labeled with DY647 (^{DY647}IFNα2 M148A) at the single-molecule level. This ligand requires simultaneous interaction with both IFNAR1 and IFNAR2 for binding to the cell-surface receptor and thus indirectly probes ternary-complex formation[22,43]. In contrast to findings from previous experiments performed in HeLa cells or IFNAR2-deficient U5A cells[22], no substantial difference in the amount of ^{DY647}IFNα2 M148A bound to the cell-surface receptor was detected in U6A cells expressing USP18 (**Fig. 6a**,**b**). This result suggests impaired negative regulation by USP18 in the absence of STAT2. By contrast, complementation by coexpression of STAT2 significantly decreased the number of ^{DY647}IFNα2 M148A on the cell surface, as expected for effective desensitization by USP18. Complementation with transiently transfected STAT2, without USP18, had no effect on ligand binding. For both CC-DB and CC fragments of STAT2, we observed substantial USP18-mediated negative regulation of ternary-complex formation, thus confirming the relevance of the STAT2-USP18 interaction in inhibiting IFNAR assembly. These results confirm that the presence of both STAT2 and USP18 is required for USP18-mediated inhibition of ternary-complex formation at the plasma membrane.

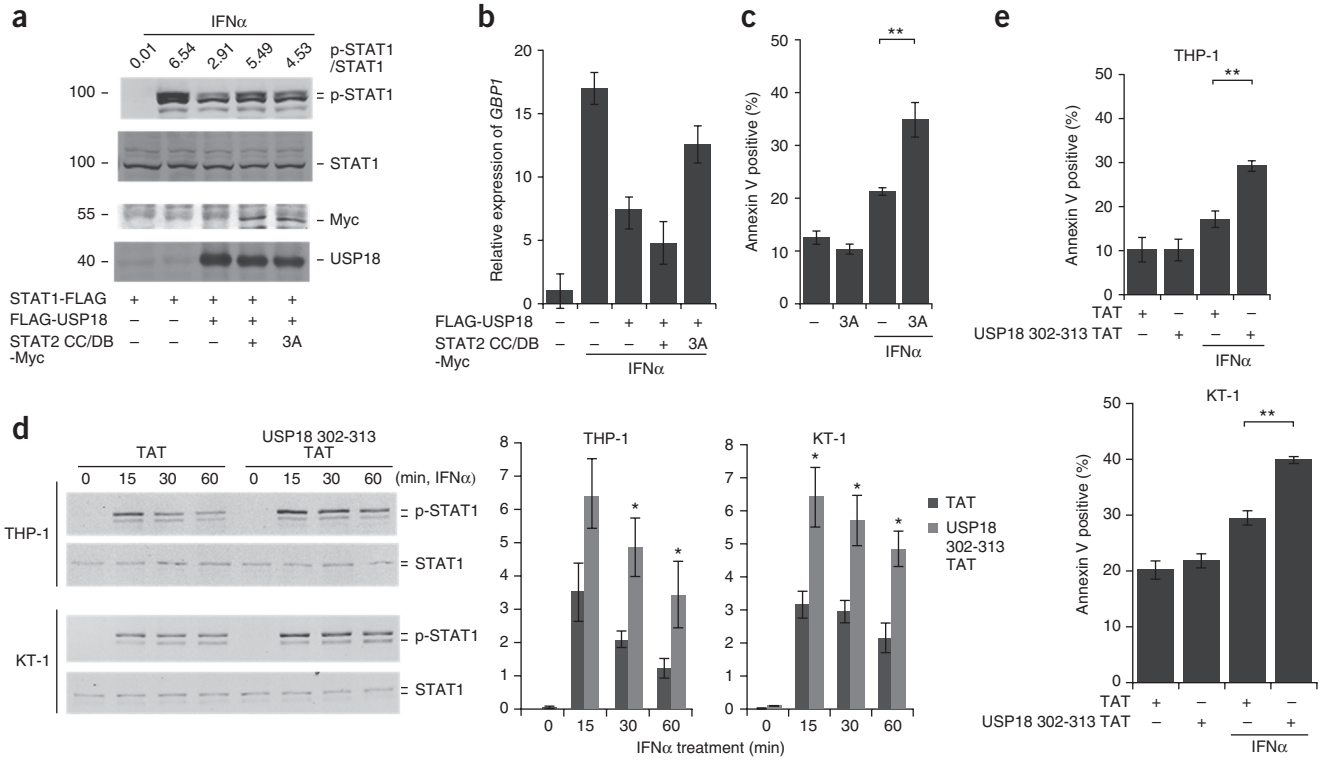

Figure 7 Inhibiting negative-feedback regulation of USP18 by targeting its interaction with STAT2. (**a**) Immunoblot analysis of 293T cells cotransfected with plasmids encoding STAT1-FLAG, FLAG-USP18 and either STAT2 CC/DB-Myc or the mutant STAT2 CC/DB L227A R409A K415A-Myc (3A). After treatment with IFNα (1,000 U/ml) for 15 min, cell lysates were collected and analyzed with the indicated antibodies. The ratio of p-STAT1 to total STAT1 was quantified with a LI-COR Odyssey system. Numbers on the left show molecular weight (kDa). (**b**) Cells described in **a** were treated with IFNα (1,000 U/ml) for 12 h, and expression of GBP1 was analyzed by qRT–PCR. Data are mean and s.d. from 2 independent experiments. (**c**) THP-1 cells transduced with either MIP control (–) or MIP-STAT2 CC/DB 3A (3A) were treated with IFNα (1,000 U/ml) for 48 h, and annexin V–positive cells were then analyzed by flow cytometry. Data are mean and s.e.m. from 3 independent experiments, performed with independently generated stable cell lines. $^{**}P < 0.01$ by two-tailed Student's *t* test. (**d**) THP-1 and KT-1 cells were treated with transactivator of transcription protein (TAT) or USP18 aa 302–313 TAT peptide. Five hours after peptide treatment, IFNα (1,000 U/ml) was added for the indicated times, and cells were analyzed by immunoblotting. The ratio of p-STAT1 to total STAT1 from 3 independent experiments was quantified (right). Data are shown as mean and s.e.m. from 3 independent experiments. $^{*}P < 0.05$ by two-tailed Student's *t* test. (**e**) TAT- or USP18 aa 302–313 TAT-peptide-treated THP-1 and KT-1 cells were incubated with IFNα (1,000 U/ml) for 48 h, and annexin V–positive cells were then analyzed by flow cytometry. Data are mean and s.e.m. from 3 independent experiments. $^{**}P < 0.01$ by two-tailed Student's *t* test.

Furthermore, we analyzed the effective cell-surface binding affinity of fluorescein isothiocyanate (FITC)-labeled IFNα to cell-surface IFNAR by flow cytometry. FITC-labeled IFNα showed concentration-dependent binding to 2fTGH cells but did not bind to IFNAR2-deficient U5A cells (**Supplementary Fig. 6a**). FITC-labeled IFNα had similar biological activity to that of nonlabeled IFNα (**Supplementary Fig. 6c**). These results demonstrate that FITC-labeled IFNα is suitable for testing the IFN-receptor interaction. In U6A cells, we ectopically expressed USP18, STAT2, and STAT2 lacking both the CC and DB domains (STAT2ΔCC/DB) and consequently lacking USP18-binding ability (**Fig. 3**). USP18 decreased IFNα binding to U6A cells only in the presence of full-length STAT2 but not STAT2ΔCC/DB (**Fig. 6c**), thus supporting the notion that interaction of STAT2 and USP18 is important for type I IFN ligand-receptor binding. Phosphorylation of Y690 in STAT2 is critical not only for ISGF3 formation and ISG regulation but also for STAT2-mediated STAT1 phosphorylation[44]. Accordingly, expression of the STAT2 Y690F mutant in U6A cells did not enhance IFNα-induced STAT1 phosphorylation (**Fig. 6d**). Because the STAT2-USP18 interaction was not affected by this mutation (**Supplementary Fig. 6d**), USP18 expression still decreased phosphorylation of STAT1 in STAT2 Y690F-expressing U6A cells stimulated with IFNα (**Fig. 6d**). Importantly, expression of USP18 also decreased the level of IFNα binding to STAT2 Y690F-expressing U6A cells (**Fig. 6e**). Together, these results establish that the interaction between USP18 and STAT2 mediates the inhibitory effect of USP18 on type I IFN receptor assembly and signaling. Our data suggest that USP18 is recruited to IFNAR2 via its interaction with the STAT2 CC and DB domains, thus allowing an additional interaction of USP18 with the membrane-proximal domain of IFNAR2 (**Fig. 6f**) and probably resulting in JAK1 dissociation[21].

Disruption of the STAT2-USP18 interaction enhances IFN-dependent response

IFNs modulate crucial immune responses during pathogen infection and against malignant cells, but these responses are effectively abrogated by the expression of USP18. Therefore, we next examined whether a peptide comprising the STAT2 CC and DB domains could block the USP18-STAT2 interaction and consequently maintain IFN signaling responses in the presence of USP18. To this end, STAT1, USP18, and the STAT2 CC/DB fragment were coexpressed in HEK 293T cells (**Fig. 7a**). As expected, STAT2 CC/DB counteracted the negative effect of USP18, thus resulting in increased STAT1 phosphorylation.

The CC domain of STAT2 interacts with IRF9, and the DB domain of STAT2 is essential for activation of ISG transcription[45,46]. Although

expression of STAT2 CC/DB successfully disrupts the STAT2-USP18 negative-feedback interaction, it may also compete with wild-type STAT2 in the formation of the ISGF3 complex and in the binding to ISRE promoter regions after nuclear translocation. To investigate these downstream biological functions, we generated a STAT2 CC/DB triple mutant (designated STAT2 CC/DB 3A) bearing L227A, R409A, and K415A substitutions. The single L227A point mutation substantially decreased interaction of STAT2 CC/DB with IRF9 (**Supplementary Fig. 7a**). Furthermore, residues R409 and K415 have been reported to be important in nuclear translocation[47]. STAT2 CC/DB 3A was therefore expected to be primarily cytosolic and to lack the ability to bind to IRF9. However, STAT2 CC/DB 3A retained the ability to disrupt the USP18 inhibitory effect on STAT1 phosphorylation (**Fig. 7a**, right lane). In addition, STAT2 CC/DB 3A, but not STAT2 CC/DB, partially blocked the effect of USP18 on transcription of ISGs, such as GBP1 and IFIT1 (**Fig. 7b** and **Supplementary Fig. 7b**). Both IFNα and IFNβ are known to promote apoptosis in several cancer cell lines[48]. Here, we found that IFNα or IFNβ treatment induced apoptosis in the human myeloid cell line THP-1, and this effect was significantly enhanced after addition of STAT2 CC/DB 3A (**Fig. 7c** and **Supplementary Fig. 7c**).

Because we identified the critical region for the USP18 interaction with STAT2 (**Supplementary Fig. 3c**), we also examined whether a peptide comprising USP18 aa 302–313 might have a similar effect as the STAT2 CC/DB domains. IFN-induced STAT1 phosphorylation in THP-1 and KT-1 cells treated with this peptide, compared with the control, was enhanced and prolonged (**Fig. 7d**). In agreement with these results, we observed enhanced GBP-1 expression and increased apoptosis in THP-1 and KT-1 cells treated with the USP18 aa 302–313 peptide (**Fig. 7e** and **Supplementary Fig. 7d**). Together, our results demonstrate that, by interfering with the USP18-STAT2 interaction, USP18-mediated inhibition of type I IFN signaling can be suppressed. This finding suggests that the STAT2-USP18 interaction interface may be a useful drug target for enhancing type I IFN responses.

DISCUSSION

Type I IFNs are involved in a variety of different processes of innate and adaptive immune responses[49,50], which are coordinated by a finely tuned regulatory signaling network[1]. Unraveling the molecular and cellular determinants governing this network will be imperative to improve understanding and to therapeutically manipulate immunological responses in a variety of disease contexts. A critical role of negative regulators in type I IFN signaling is emerging[15]; these negative regulators have been targeted by inhibitors to enhance the IFN response: PKD2 exerts negative feedback via IFNAR1 (ref. 51), but the PKD inhibitor CID755673 only slightly prolongs the IFN response. SOCS1 and SOCS3 inhibit tyrosine phosphorylation and nuclear translocation of STAT1 by binding to JAKs[52]. However, inhibition of SOCS1 only transiently enhances the IFN response, because it is expressed in the early phase after type I IFN treatment and is undetectable later on[53]. Additionally, SOCS1 affects not only type I but also type II IFN signaling. In contrast, inhibition of USP18 leads to enhanced type I IFN signaling at an early stage[21] and produces a prolonged response at later stages[27,54]. Therefore, we explored the specific mechanism of signal inhibition by the STAT2-USP18 negative-feedback interaction.

STAT2 is well known as a unique effector of type I and type III IFN signaling that not only is an integral component of the ISGF3 complex responsible for the induction of ISGs[55,56] but also positively regulates STAT1 phosphorylation[38,57]. The biological importance of STAT2 in type I IFN signaling has been further corroborated by the study of STAT2-deficient humans and mice, which become immune compromised and are vulnerable to viral infection[39,58]. However, the present study provides what is, to our knowledge, the first evidence that USP18 requires STAT2 for exerting its inhibitory effect on IFN signaling. USP18 decreased IFN binding and receptor dimerization as well as JAK1 phosphorylation only when STAT2 was present. These observations establish the key role of STAT2 in USP18-mediated inhibition of IFN signaling and moreover suggest that the increased STAT2 levels induced by IFN signaling may further enhance negative feedback by USP18.

To fulfill its inhibitory function, USP18 must be recruited to the receptor[21]. Previously, we have reported that USP18 interferes with the recruitment of IFNAR1 to the IFN–IFNAR1–IFNAR2 ternary complex, through an unknown mechanism[22]. Here, we demonstrated that STAT2 acts as an adaptor recruiting USP18 to IFNAR2 via its membrane-distal constitutive binding site for STAT2. Binding of STAT2 and USP18 to IFNAR2 is synergistic, in line with a previous observation that the STAT2-IFNAR2 interaction is strengthened by USP18 (ref. 33). Hence, through stabilizing the interaction between STAT2 and IFNAR2, USP18 may also negatively regulate the STAT phosphorylation process by decreasing the STAT-phosphorylation turnover rate and the activation of the ISGF3 complex. We assume that recruitment of USP18 to IFNAR2 via STAT2 promotes the otherwise weak interaction of USP18 with a membrane-proximal site of IFNAR2. We have previously shown that this interaction competes with JAK1 binding, thus effectively decreasing ternary-complex formation and signal activation at the plasma membrane; these two roles are probably the main inhibitory functions of USP18 (refs. 21–23). Here, we found that STAT2 interacts with the N- as well as the C-terminal regions of USP18. In agreement with previous results[21], our experiments confirmed that the N- and C-terminal regions of USP18 directly interact with IFNAR2. Together, our data suggest that USP18 simultaneously interacts with IFNAR2 via STAT2 in the membrane-distal region and directly in the membrane-proximal region (**Fig. 6f**).

Both the CC and DB domains of STAT2 are critical for the interaction with USP18 and for USP18-mediated negative-feedback regulation of type I IFN signaling, as determined on the basis of type I IFN binding and STAT phosphorylation. Interestingly, these domains are also critical for STAT2 interaction with IFNAR2, thereby explaining the binding synergy, and moreover tightly linking STAT2 and USP18 functions. Indeed, we demonstrated that a construct containing only the STAT2 CC/DB had an inhibitory effect on the function of USP18 and consequently increased STAT1 phosphorylation. Notably, our results revealed that the USP18 302–313 peptide disrupted the USP18-STAT2 interaction interface. Both peptides significantly enhanced IFN-triggered responses. Notably, although this inhibitory effect was strong, it was not complete, thus indicating either that other factors are involved or that there is room for improving these inhibitors. Further studies will be required to unravel the STAT2 CC/DB and USP18 aa 302–313 inhibitory effect on USP18 function, including a structural analysis using purified proteins when they become available. Thus, novel strategies to manipulate negative feedback by USP18 by use of small-molecule PPI modulators, which are currently emerging[59], may be possible.

Importantly, USP18 has a negative role not only in type I but also in type III IFN signaling[60], and this role also involves STAT2. Therefore, a similar mechanism of negative regulation by USP18 and STAT2 in type III IFN signaling can be expected. Indeed, preliminary data from our laboratory show that USP18 binds type III IFN receptor IL-28RA and has no inhibitory effect on type III IFN signaling in U6A cells

(K.-I.A. and D.-E.Z., unpublished data). Although our current functional peptide studies presented in **Figure 7** still lack *in vivo* validation, the tight functional linkage of STAT2 and USP18 has evolved to warrant efficient control of ISGF3-based gene expression. Design of modulators for controlling the USP18-STAT2 interaction may therefore yield the ability to enhance or diminish type I and type III IFN responses in therapeutic settings.

METHODS

Methods, including statements of data availability and any associated accession codes and references, are available in the online version of the paper.

Note: Any Supplementary Information and Source Data files are available in the online version of the paper.

ACKNOWLEDGMENTS

We thank A. Garcia-Sastre (Icahn School of Medicine at Mount Sinai) for *Stat2*$^{-/-}$ MEFs, D. Cheresh (Moores UCSD Cancer Center) for MDA-MB-231, G. Stark (Cleveland Clinic) for sharing U-series cell lines, S. Fujita (Ehime University School of Medicine) for KT-1 cells, R. Xiang (The Scripps Research Institute) for WEHI-3B cells, S. Urbe (University of Liverpool) for GFP-fusion STAT2 and USP18 constructs, V. Verkhusha (Albert Einstein College of Medicine) for the mTag-BFP construct, T. Akagi (KAN Research Institute) for providing pCX4-series vectors, S. Kotenko (Rutgers New Jersey Medical School) for the pcDEF-hIFNAR2 DNA construct, D. Baker (Biogen Idec) for supplying recombinant human IFNβ and anti–human IFNAR1 antibody, the staff of Hybrigenics for their contribution, G. Hikade for technical support, and R. Kurre for advice on fluorescence microscopy. This study was supported by NIH R01HL091549 and R01CA177305 to D.-E.Z. and SFB 944 from the DFG to J.P. and J.J.H.

AUTHOR CONTRIBUTIONS

K.A., S.L., and S.A.S. designed, performed, and analyzed experiments, and wrote the manuscript; C.B., Y.Z., S.M., J.-B.F., S.W., J.J.H., Z.L., M.Y., S.P., and F.C. performed experiments or provided critical information; J.P. and D.-E.Z. conceived the project, designed experiments, analyzed experimental data, and wrote the manuscript.

COMPETING FINANCIAL INTERESTS

The authors declare no competing financial interests.

1. Hertzog, P.J. & Williams, B.R. Fine tuning type I interferon responses. *Cytokine Growth Factor Rev.* **24**, 217–225 (2013).
2. Schneider, W.M., Chevillotte, M.D. & Rice, C.M. Interferon-stimulated genes: a complex web of host defenses. *Annu. Rev. Immunol.* **32**, 513–545 (2014).
3. Ivashkiv, L.B. & Donlin, L.T. Regulation of type I interferon responses. *Nat. Rev. Immunol.* **14**, 36–49 (2014).
4. Zitvogel, L., Galluzzi, L., Kepp, O., Smyth, M.J. & Kroemer, G. Type I interferons in anticancer immunity. *Nat. Rev. Immunol.* **15**, 405–414 (2015).
5. Borden, E.C. *et al.* Interferons at age 50: past, current and future impact on biomedicine. *Nat. Rev. Drug Discov.* **6**, 975–990 (2007).
6. Sistigu, A. *et al.* Cancer cell-autonomous contribution of type I interferon signaling to the efficacy of chemotherapy. *Nat. Med.* **20**, 1301–1309 (2014).
7. Rieger, P.T. Interferon-alpha: a clinical update. *Cancer Pract.* **3**, 356–365 (1995).
8. Dusheiko, G. Side effects of alpha interferon in chronic hepatitis C. *Hepatology* **26** (Suppl.1), S112–S121 (1997).
9. Crow, Y.J. Aicardi-Goutières syndrome. *Handb. Clin. Neurol.* **113**, 1629–1635 (2013).
10. Meyer, O. Interferons and autoimmune disorders. *Joint Bone Spine* **76**, 464–473 (2009).
11. Uzé, G., Lutfalla, G. & Mogensen, K.E. Alpha and beta interferons and their receptor and their friends and relations. *J. Interferon Cytokine Res.* **15**, 3–26 (1995).
12. Li, X., Leung, S., Qureshi, S., Darnell, J.E. Jr. & Stark, G.R. Formation of STAT1-STAT2 heterodimers and their role in the activation of IRF-1 gene transcription by interferon-alpha. *J. Biol. Chem.* **271**, 5790–5794 (1996).
13. Platanias, L.C. Mechanisms of type-I- and type-II-interferon-mediated signalling. *Nat. Rev. Immunol.* **5**, 375–386 (2005).
14. van Boxel-Dezaire, A.H., Rani, M.R. & Stark, G.R. Complex modulation of cell type-specific signaling in response to type I interferons. *Immunity* **25**, 361–372 (2006).
15. Porritt, R.A. & Hertzog, P.J. Dynamic control of type I IFN signalling by an integrated network of negative regulators. *Trends Immunol.* **36**, 150–160 (2015).
16. Marchetti, M. *et al.* Stat-mediated signaling induced by type I and type II interferons (IFNs) is differentially controlled through lipid microdomain association and clathrin-dependent endocytosis of IFN receptors. *Mol. Biol. Cell* **17**, 2896–2909 (2006).
17. Schreiber, G. & Piehler, J. The molecular basis for functional plasticity in type I interferon signaling. *Trends Immunol.* **36**, 139–149 (2015).
18. Liu, L.Q. *et al.* A novel ubiquitin-specific protease, UBP43, cloned from leukemia fusion protein AML1-ETO-expressing mice, functions in hematopoietic cell differentiation. *Mol. Cell. Biol.* **19**, 3029–3038 (1999).
19. Schwer, H. *et al.* Cloning and characterization of a novel human ubiquitin-specific protease, a homologue of murine UBP43 (Usp18). *Genomics* **65**, 44–52 (2000).
20. Malakhov, M.P., Malakhova, O.A., Kim, K.I., Ritchie, K.J. & Zhang, D.E. UBP43 (USP18) specifically removes ISG15 from conjugated proteins. *J. Biol. Chem.* **277**, 9976–9981 (2002).
21. Malakhova, O.A. *et al.* UBP43 is a novel regulator of interferon signaling independent of its ISG15 isopeptidase activity. *EMBO J.* **25**, 2358–2367 (2006).
22. Wilmes, S. *et al.* Receptor dimerization dynamics as a regulatory valve for plasticity of type I interferon signaling. *J. Cell Biol.* **209**, 579–593 (2015).
23. François-Newton, V. *et al.* USP18-based negative feedback control is induced by type I and type III interferons and specifically inactivates interferon α response. *PLoS One* **6**, e22200 (2011).
24. Zhang, X. *et al.* Human intracellular ISG15 prevents interferon-α/β over-amplification and auto-inflammation. *Nature* **517**, 89–93 (2015).
25. Meuwissen, M.E. *et al.* Human USP18 deficiency underlies type 1 interferonopathy leading to severe pseudo-TORCH syndrome. *J. Exp. Med.* **213**, 1163–1174 (2016).
26. Ritchie, K.J. *et al.* Role of ISG15 protease UBP43 (USP18) in innate immunity to viral infection. *Nat. Med.* **10**, 1374–1378 (2004).
27. Kim, K.I. *et al.* Enhanced antibacterial potential in UBP43-deficient mice against *Salmonella typhimurium* infection by up-regulating type I IFN signaling. *J. Immunol.* **175**, 847–854 (2005).
28. Honke, N. *et al.* Enforced viral replication activates adaptive immunity and is essential for the control of a cytopathic virus. *Nat. Immunol.* **13**, 51–57 (2011).
29. Honke, N. *et al.* Usp18 driven enforced viral replication in dendritic cells contributes to break of immunological tolerance in autoimmune diabetes. *PLoS Pathog.* **9**, e1003650 (2013).
30. Goldmann, T. *et al.* USP18 lack in microglia causes destructive interferonopathy of the mouse brain. *EMBO J.* **34**, 1612–1629 (2015).
31. Ketscher, L. *et al.* Selective inactivation of USP18 isopeptidase activity *in vivo* enhances ISG15 conjugation and viral resistance. *Proc. Natl. Acad. Sci. USA* **112**, 1577–1582 (2015).
32. Yim, H.Y. *et al.* Elevated response to type I IFN enhances RANKL-mediated osteoclastogenesis in Usp18-knockout mice. *J. Immunol.* **196**, 3887–3895 (2016).
33. Löchte, S., Waichman, S., Beutel, O., You, C. & Piehler, J. Live cell micropatterning reveals the dynamics of signaling complexes at the plasma membrane. *J. Cell Biol.* **207**, 407–418 (2014).
34. Levy, D.E. & Darnell, J.E. Jr. Stats: transcriptional control and biological impact. *Nat. Rev. Mol. Cell Biol.* **3**, 651–662 (2002).
35. Ketscher, L. & Knobeloch, K.P. ISG15 uncut: dissecting enzymatic and non-enzymatic functions of USP18 in vivo. *Cytokine* **76**, 569–571 (2015).
36. Pellegrini, S., John, J., Shearer, M., Kerr, I.M. & Stark, G.R. Use of a selectable marker regulated by alpha interferon to obtain mutations in the signaling pathway. *Mol. Cell. Biol.* **9**, 4605–4612 (1989).
37. Rani, M.R. *et al.* Characterization of beta-R1, a gene that is selectively induced by interferon beta (IFN-beta) compared with IFN-alpha. *J. Biol. Chem.* **271**, 22878–22884 (1996).
38. Leung, S., Qureshi, S.A., Kerr, I.M., Darnell, J.E. Jr. & Stark, G.R. Role of STAT2 in the alpha interferon signaling pathway. *Mol. Cell. Biol.* **15**, 1312–1317 (1995).
39. Hambleton, S. *et al.* STAT2 deficiency and susceptibility to viral illness in humans. *Proc. Natl. Acad. Sci. USA* **110**, 3053–3058 (2013).
40. Yang, E., Wen, Z., Haspel, R.L., Zhang, J.J. & Darnell, J.E. Jr. The linker domain of Stat1 is required for gamma interferon-driven transcription. *Mol. Cell. Biol.* **19**, 5106–5112 (1999).
41. Nguyen, V.P. *et al.* Stat2 binding to the interferon-alpha receptor 2 subunit is not required for interferon-alpha signaling. *J. Biol. Chem.* **277**, 9713–9721 (2002).
42. Li, X., Leung, S., Kerr, I.M. & Stark, G.R. Functional subdomains of STAT2 required for preassociation with the alpha interferon receptor and for signaling. *Mol. Cell. Biol.* **17**, 2048–2056 (1997).
43. Piehler, J., Roisman, L.C. & Schreiber, G. New structural and functional aspects of the type I interferon-receptor interaction revealed by comprehensive mutational analysis of the binding interface. *J. Biol. Chem.* **275**, 40425–40433 (2000).
44. Improta, T. *et al.* Transcription factor ISGF-3 formation requires phosphorylated Stat91 protein, but Stat113 protein is phosphorylated independently of Stat91 protein. *Proc. Natl. Acad. Sci. USA* **91**, 4776–4780 (1994).
45. Martinez-Moczygemba, M., Gutch, M.J., French, D.L. & Reich, N.C. Distinct STAT structure promotes interaction of STAT2 with the p48 subunit of the interferon-alpha-stimulated transcription factor ISGF3. *J. Biol. Chem.* **272**, 20070–20076 (1997).

46. Brierley, M.M. & Fish, E.N. Functional relevance of the conserved DNA-binding domain of STAT2. *J. Biol. Chem.* **280**, 13029–13036 (2005).
47. Melen, K., Kinnunen, L. & Julkunen, I. Arginine/lysine-rich structural element is involved in interferon-induced nuclear import of STATs. *J. Biol. Chem.* **276**, 16447–16455 (2001).
48. Chawla-Sarkar, M., Leaman, D.W. & Borden, E.C. Preferential induction of apoptosis by interferon (IFN)-beta compared with IFN-alpha2: correlation with TRAIL/Apo2L induction in melanoma cell lines. *Clin. Cancer Res.* **7**, 1821–1831 (2001).
49. González-Navajas, J.M., Lee, J., David, M. & Raz, E. Immunomodulatory functions of type I interferons. *Nat. Rev. Immunol.* **12**, 125–135 (2012).
50. Chen, H.M. *et al.* Critical role for constitutive type I interferon signaling in the prevention of cellular transformation. *Cancer Sci.* **100**, 449–456 (2009).
51. Zheng, H., Qian, J., Baker, D.P. & Fuchs, S.Y. Tyrosine phosphorylation of protein kinase D2 mediates ligand-inducible elimination of the Type 1 interferon receptor. *J. Biol. Chem.* **286**, 35733–35741 (2011).
52. Yoshimura, A., Naka, T. & Kubo, M. SOCS proteins, cytokine signalling and immune regulation. *Nat. Rev. Immunol.* **7**, 454–465 (2007).
53. Sarasin-Filipowicz, M. *et al.* Alpha interferon induces long-lasting refractoriness of JAK-STAT signaling in the mouse liver through induction of USP18/UBP43. *Mol. Cell. Biol.* **29**, 4841–4851 (2009).
54. Zou, W. *et al.* Microarray analysis reveals that Type I interferon strongly increases the expression of immune-response related genes in Ubp43 (Usp18) deficient macrophages. *Biochem. Biophys. Res. Commun.* **356**, 193–199 (2007).
55. Kotenko, S.V. *et al.* IFN-λs mediate antiviral protection through a distinct class II cytokine receptor complex. *Nat. Immunol.* **4**, 69–77 (2003).
56. Brierley, M.M., Marchington, K.L., Jurisica, I. & Fish, E.N. Identification of GAS-dependent interferon-sensitive target genes whose transcription is STAT2-dependent but ISGF3-independent. *FEBS J.* **273**, 1569–1581 (2006).
57. Au-Yeung, N., Mandhana, R. & Horvath, C.M. Transcriptional regulation by STAT1 and STAT2 in the interferon JAK-STAT pathway. *JAK-STAT* **2**, e23931 (2013).
58. Park, C., Li, S., Cha, E. & Schindler, C. Immune response in Stat2 knockout mice. *Immunity* **13**, 795–804 (2000).
59. London, N., Raveh, B. & Schueler-Furman, O. Druggable protein-protein interactions: from hot spots to hot segments. *Curr. Opin. Chem. Biol.* **17**, 952–959 (2013).
60. Burkart, C. *et al.* Usp18 deficient mammary epithelial cells create an antitumour environment driven by hypersensitivity to IFN-λ and elevated secretion of Cxcl10. *EMBO Mol. Med.* **5**, 1035–1050 (2013).

ONLINE METHODS

Yeast two-hybrid screen. cDNA encoding full-length human USP18 (wild-type and C64A-mutated form) were cloned into the LexA DNA-binding-domain plasmid derived from pBTM116 and used as bait in yeast two-hybrid screens of a human placental cDNA library (complexity of 10^6 colonies), as previously described[61]. A total of 11 independent clones displaying similarity to STAT2 proteins were isolated.

Yeast two-hybrid assay. To confirm specific interactions, the following yeast two-hybrid vectors were created, which contained Gal4 DNA-binding and activation domains: pGBD-C1 (vector control), DNA-binding-domain fusions pJJH1722 (pGBD-STAT2) and pJJH1719 (pGBD-USP18); and pGAD424A (vector control), pJJH1721 (pGAD-STAT2) and pJJH1720 (pGAD-USP18) for expression of activation-domain fusion proteins. Complete sequences of these plasmids are available upon request. For two-hybrid analyses with these constructs, the *Saccharomyces cerevisiae* strains pJ69-4a and pJ69-4α were used[62]. Three microliters of overnight cultures from strains pJ69-4a/pJ69-4α carrying two-hybrid plasmids with the indicated coding sequences were spotted onto selective medium for plasmid maintenance and incubated for 10 d.

Plasmid construction. Human STAT2 and its mutant cDNAs were cloned into the pcDNA3.1 vector. Human STAT2 was also cloned into the pCAG and GST (6p-1) vector. Mouse Stat2 was cloned into the MSCV-IRES-Puro (MIP) retroviral vector. shRNA plasmids (pLKO.1 vectors) for mouse Stat2 (TRCN0000081538-0000081542) and control were purchased from Dharmacon.

Human USP18 and its mutant cDNAs were cloned into the pcDNA3.1, pCMV7.1 3× FLAG, pEGFP-C1, and MIP vectors. Mouse Usp18 was cloned into the pCX4-bsr retroviral vector. Plasmid encoding human IFNAR2 in the pcDEF3 vector was kindly provided by S. Kotenko. Human IFNAR2 was also cloned into the pCAG and pEBG vectors.

Monomeric GFP, human STAT2-mEGFP, and human mEGFP-USP18 fusion constructs (kind gift from Sylvie Urbé[63]) were cloned into the plasmid vector pSEMS-26m (Covalys) for expression in mammalian cells. Monomeric EGFP was obtained through A206K mutation within the EGFP sequence of pEGFP-N1 (Clontech). An artificial transmembrane domain (TMD) with the extracellular sequence ASALAALAALAALAALAALAALAKSSRL (with ALA7 underlined) (as described in ref. 64) extracellularly fused to a HaloTag (Promega) and mTagBFP (obtained from V. Verkhusha[65]) sequences and intracellularly fused to human STAT2 was cloned into pDisplay (Invitrogen).

For cloning of pSEMS-HaloTag-IFNAR2, the gene encoding the HaloTag followed by the genes encoding full length IFNAR2 or IFNAR2Δ375 without the N-terminal signal sequences were inserted into pDisplay (Invitrogen). The constructs including the Igκ signal sequence from the pDisplay vector were transferred by restriction with EcoRI and NotI into pSems-26m. The genes encoding mTagBFP, HaloTag and IFNAR2 were inserted into pDisplay-HaloTag to generate the construct pDisplay-HaloTag-mTagBFP-IFNAR2.

Cell culture and primary bone-marrow cells from *Usp18*$^{-/-}$ mice. HEK293T (ATCC), HeLa (ATCC), MDA-MB-231 (kindly provided previously by D. Cheresh), *Stat2*$^{-/-}$ MEF (kindly provided by A. Garcia-Sastre), and U-series (2fTGH, U1A, U2A, U4A, U5A, and U6A) (kindly provided by G. Stark) cells were grown in DMEM supplemented with glutamine, penicillin/streptomycin, and 10% FBS. THP-1 (ATCC) and KT-1 cells (kindly provided previously by S. Fujita) were grown in RPMI medium supplemented with glutamine, penicillin/streptomycin, and 10% FBS. Ba/F3 cells were grown in RPMI1640 medium supplemented with 15% FBS and 5% conditional medium from WEHI-3B cells (kindly provided previously by R. Xiang). Bone-marrow cells from *Usp18*$^{-/-}$ (ref. 66) mice were grown in RPMI1640 medium supplemented with 20% FBS and IL3 and SCF conditional medium. HeLa and U-series cells were routinely tested for mycoplasma. All the procedures for *Usp18*$^{-/-}$ mice experiments were approved by the UCSD Institutional Animal Care and Use Committee.

Transfection and lentivirus or retrovirus infection. Transfection was conducted with PEI (polyethylenimine)[67]. For the retrovirus or lentivirus production, 293T cells were cotransfected with plasmids encoding viral vectors and packaging vectors pCL-10A1 for human cells or Ecopac for mouse cells. Viral particles were collected 48 h after transfection and filtered with an 0.45-μm sterile filter. For the retrovirus or lentivirus infection, spin infection (2,000*g*, 3 h, 30 °C; Allegra X12R (Beckman Coulter)) in the presence of polybrene (8 μg/ml) was performed.

Reagents and antibodies. Commercial antibodies used were: anti-phospho-JAK1 (Tyr1022/1023; Cell Signaling, 3331), anti-JAK1 (Cell Signaling, 3332), anti-phospho-STAT1 (Tyr701; Cell Signaling, 9167), anti- STAT1 (Cell Signaling, 9172), anti-STAT2 (Santa Cruz, sc-22816), anti–green fluorescent protein (anti-GFP, Invitrogen, A11122), anti-tubulin (Sigma, T9026), anti-FLAG (Sigma, F1804), anti-Myc (Santa Cruz, sc-40), anti-hemagglutinin (HA; Roche 12CA5 or 3F10), anti-IFNAR1 (Biogen Idec, AA3), and anti-IFNAR2 FITC (Sino Biological, 10359-H08H). Validation information is available from the vendors. Anti-USP18 antibody was as previously described[60].

Recombinant human IFNβ was provided from Biogen Idec. Recombinant human IFNα, mouse IFNβ, and human IFNλ were purchased from Peprotech. Recombinant IFNα2 and the mutant IFNα2-M148A used in cell micropatterning and single-molecule assays was produced in *Escherichia coli* and purified as previously described[43]. For site-specific fluorescent labeling, IFNα2 and the mutant IFNα2-M148A fused to an N-terminal ybbR tag were produced in *E. coli* and conjugated with DY 647 as previously described[68]. A degree of labeling >90% was obtained, as determined by UV/vis spectroscopy.

The RGD peptide Ac-CGRGDS-COOH was custom synthesized by Coring System Diagnostix. Poly-L-lysine (PLL) hydrobromide (MW, 15,000–30,000 g/mol) was purchased from Sigma-Aldrich. Homobifunctional dicarboxy-PEG (COOH-PEG3000-COOH, MW of PEG, 3,000 g/mol) was from Rapp Polymere. Poly-L-lysine graft-modified with methoxy-PEG (MW, 2,000 g/mol) (PLL-PEG-OMe) was purchased from SuSoS AG. HaloTag-O2-amine ligand (HTL) was purchased from Promega. Dimethylformamide (DMF), *N*-ethyldiisopropylamine (DIPEA), *N*,*N*′-diisopropylcarbodiimide (DIC), and *N*-(3-dimethylaminopropyl)-*N*′-ethyl-carbodiimide hydrochloride (EDC) were purchased from Sigma-Aldrich.

Synthesis of functionalized poly-L-lysine-graft-(polyethylene glycol) copolymer (PLL-PEG derivatives, PLL-PEG-HTL and PLL-PEG-RGD) was carried out as previously described[69].

RNA isolation and qRT–PCR analysis. RNA was extracted with TRIzol (Thermo Fisher Scientific). For qRT–PCR analyses, equal amounts of RNA were reverse-transcribed with qScript (Quanta Biosciences), and the resulting cDNA templates were subjected to qRT–PCR with a KAPA SYBR FAST universal qPCR kit (Kapa Biosystems) and CFX96 thermal cycler (Bio-Rad).

The primer sequences were as follows:

RT-*Isg15*-Fw, GACTAACTCCATGACGGTG; RT-*Isg15*-Rev, AACTGGTC TTCGTGACTTG

RT-*Gbp1*-Fw, GGAGGCCATTGAGGTCTTCAT; RT-*Gbp1*-Rev, CAAAGG CATCTCGTTTGGCT

RT-*Cxcl9*-Fw, TCCTTTTGGGCATCATCTTCC; RT-*Cxcl9*-Rev, TTTGTAG TGGATCGTGCCTCG

RT-*Irf9*-Fw, GCCTTTGCCCCATCCCCATCTC; RT-*Irf9*-Rev, CCCCTGG CCCTGGAAGTACTGG

RT-*Ifit1*-Fw; TGGCGACCTGGGGCAACTGTG; RT-*Ifit1*-Rev, TGGGCTG CCTGTTTCGGGATGTC

RT-*Igtp*-Fw; CGCCTCATCAGCCCGTGGTCTAA; RT-*Igtp*-Rev, TGCCATT GCCAGAGTCCCCAGTC

RT-*GBP1*-Fw, CCAGTTGCTGAAAGAGCAAGAGA; RT-*GBP1*-Rev, TCCC TCTTTTAGTAGTTGCTCCTGTT

RT-*IFIT1*-Fw,AAGGCAGGCTGTCCGCTTA; RT-*IFIT1*-Rev, TCCTGTCC TTCATCCTGAAGCT

Immunoblotting. Immunoblotting was performed as previously described in detail[70]. All samples were denatured in 1× sample buffer (50 mM Tris-HCl, pH 6.8, 2% SDS, 2-mercaptethanol, 10% glycerol, and 1% bromophenol blue) for 5 min at 100 °C. Cells were lysed in RIPA buffer composed of 25 mM Tris-HCl, pH 8.0, 150 mM NaCl, 1 mM EDTA, 1 mM DTT, 0.1% SDS, 1% Nonidet P-40 and 0.5% sodium deoxycholate. To analyze immune complexes for coimmunoprecipitation assays, cells were lysed in binding buffer containing 25 mM Tris-HCl, pH 8.0, 150 mM NaCl, 1 mM EDTA and 0.5% Nonidet P-40 for coimmunoprecipitation assays. The cell lysates were centrifuged (15,000 r.p.m.) at 4 °C for 5 min. All lysis buffers in this study contained proteinase and phosphatase inhibitors (Roche). Soluble fractions were precleared with Protein G–Sepharose at 4 °C for 15 min.

doi:10.1038/nsmb.3378

Precleared cell lysates were immunoprecipitated for 1–4 h with the indicated antibodies. Immunocomplexes were adsorbed to the protein G–Sepharose and, after being washed three times, were eluted by boiling for 5 min. FLAG-tagged proteins were immunoprecipitated with anti-FLAG M2-agarose (Sigma). All assays were performed two to four times, and representative blots are presented. Uncropped images for immunoblots are shown in **Supplementary Data Set 1**. For the quantification, signals were detected with a LI-COR Odyssey system.

Cell micropatterning. Micropatterned surfaces were fabricated by microcontact printing. Poly(dimethylsiloxane) (PDMS) stamps were generated from basic elastomer (Sylgard 184, Dow Chemicals) mixed with curing agent (Dow Chemicals) in a 10:1 ratio and applied to a silicon master at 80 °C overnight. The silicon master, containing an array of lines with a width of 5 µm, a spacing of 10 µm and a depth of 3 µm, was generated by photolithography with a custom-designed beam mask (NB Technologies).

Standard glass coverslides for fluorescence microscopy were cleaned in a plasma cleaner for 10 min, and the stamp was then inked with 0.5 mg/ml PLL-g-PEG-HTL in PBS buffer for 10 min. For PLL-g-PEG-HTL transfer, stamps were placed onto the glass coverslides for 10 min to generate HTL patterns. After removal of the stamps, the coverslides were incubated with a mixture of 0.002 mg/ml PLL-g-PEG-RGD and 0.1 mg/ml PLL-PEG-MeO in PBS buffer for 1 min to backfill the uncoated area and to allow cell adhesion. The surface was then rinsed in Milli-Q water and dried under N_2.

For cellular micropatterning, cells were cultivated at 37 °C and 5% CO_2 in MEM supplemented with 10% FCS (MEM/FCS), 1% HEPES buffer and 1% non-essential amino acids. For transfection, cells were plated in 60-mm cell culture dishes to a density of approximately 50% confluence. One day after seeding, cells were transfected via calcium phosphate precipitation, as previously described[71]. After 24–36 h, cells were plated on chemically modified cover glasses for 15–20 h with medium containing penicillin and streptomycin (PAA). For labeling of micropatterned IFNAR, cells were incubated in the presence of 10 nM fluorescently labeled interferon coupled to ATTO655 (^{AT655}IFNα2).

Fluorescence imaging. Total internal reflection fluorescence microscopy (TIRFM) was performed with an inverted microscope (Olympus IX81) equipped with a four-line TIRF condenser (Olympus cell^TIRF MITICO), a back-illuminated electron-multiplied (EM) CCD camera (C9100-13, 512 × 512 pixel from Hamamatsu) as well as lasers at 405 nm (100 mW), 488 nm (150 mW), 561 nm (150 mW) and 640 nm (140 mW). A 60× objective with a numerical aperture of 1.49 (UAPON 60×/1.49, Olympus) or a 150× objective with a numerical aperture of 1.45 (UAPON 60×/1.45, Olympus) was used for TIRF excitation.

The excitation beam was reflected into the objective by a quad-band dichroic mirror (HC-BS R405/488/561/635, AHF), and the fluorescence was detected through a quad-band-pass filter (BrightLine HC 446/523/500/677). For multicolor experiments, a QuadView (QV2, Photometrics) equipped with suitable dichroic beamsplitters (480 dcxr, 565 dcxr, and 640 dcxr, Chroma) and emission filters (BrightLine HC 438/24, AHF; BrightLine HC 520/35, AHF; EmitterHQ 600/30, AHF; and BrightLine HC 685/40, Chroma) were used to avoid spectral cross-talk. Data acquisition was performed with the acquisition software Olympus Xcellence rt Version 1.2.

Fluorescence recovery after photobleaching (FRAP) experiments were performed at 37 °C in an incubation chamber (Olympus) with a 150× TIRF objective with a numerical aperture of 1.49 (UAPON 150×/1.49, Olympus) for TIR excitation. A circular area with a diameter of 8 µm was bleached by 405-nm excitation for 5 s with a laser power of 7.5 mW, and this was followed by acquisition with a cycle time of 1–5 s with a 1-mW 488-nm or 561-nm laser excitation.

Data analysis. Image analysis and image processing were performed with ImageJ (NIH). Image processing comprises cropping, scaling, and rotation, as well as adjustment of brightness and contrast levels. The fluorescence contrast of patterned proteins inside versus outside the pattern was calculated from the average fluorescence intensities of the bait and prey proteins obtained from rectangular ROIs by using the 'Measure' function in ImageJ. The fluorescence contrast C of the bait proteins was calculated as

$$C_{bait} = \frac{I_{bait,in} - I_{bait,out}}{I_{bait,in} - I_{bg}}$$

where $I_{bait,in}$ denotes the mean pixel intensities from selected areas inside the pattern, $I_{bait,out}$ denotes the mean pixel intensities from selected areas outside the pattern, and I_{bg} denotes the background intensity from the glass surface obtained from an ROI outside the cells. C_{bait} reflects the relative enrichment of the bait proteins and the maximal enrichment that can be achieved by the prey proteins. The contrast of the prey proteins, C_{prey}, was obtained from the background-corrected mean pixel intensities from selected areas inside and outside the pattern, as:

$$C_{prey} = \frac{I_{prey,in} - I_{bg}}{I_{prey,out} - I_{bg}}$$

Because C_{prey} varies in proportion to C_{bait}, C_{prey} was corrected to:

$$C_{prey,corr} = \frac{C_{prey}}{C_{bait}}$$

For quantitative analysis, data were visualized in box plots indicating the data distribution of the first and third quartiles (box limits), median (line), mean (open squares), and whiskers (1.5× interquartile range). Outliers are plotted as individual points.

For analysis of FRAP experiments, a rectangular region of interest within the bleached area of the pattern and a rectangular or circular ROI within the bleached area but outside the patterned area were chosen to obtain intensity values per pixel over time. FRAP curves were obtained with the following equation:

$$f = \frac{\left(F_{ROI,inside} - F_{offset}\right) - \left(F_{ROI,outside} - F_{offset}\right)}{\left[\frac{\left(F_{ref} - F_{offset}\right)}{\left(F_{ref,prebleach} - F_{offset}\right)}\right]}$$

The offset intensity (F_{offset}) was determined from an ROI outside of the cell and was subtracted by all intensity values. Free cytoplasmic diffusion in living cells was consistent both inside and outside the pattern, and its effect on FRAP was determined as ($F_{ROI,outside} - F_{offset}$). Thus the unbiased fluorescence recovery inside the pattern was obtained by the subtraction of the recovery outside the pattern as ($F_{ROI,inside} - F_{offset}$) – ($F_{ROI,outside} - F_{offset}$). A normalization factor of

$$\left[\frac{\left(F_{ref} - F_{offset}\right)}{\left(F_{ref,prebleach} - F_{offset}\right)}\right]$$

was implemented to correct background photobleaching during FRAP experiments. For this purpose, a rectangular ROI in a not-bleached patterned region was assigned as a reference, and the sequential intensities in this area were normalized to the original intensity. The recovery of the fluorescence intensity was fitted with a simple monoexponential function[72,73].

Single-molecule ligand binding assay. Single-molecule ligand binding experiments were performed in the presence of 2 nM ^{DY647}IFNα2 M148A and after an incubation time of 10 min through TIRF imaging, as described previously. All binding experiments were carried out with medium complemented with oxygen scavenger (0.5 mg ml^{-1} glucose oxidase (Sigma), 0.04 mg ml^{-1} catalase (Roche Applied Science), 5% (w/v) glucose, 1 µM ascorbic acid and 1 µM methyl viologen) to minimize photobleaching[74]. To minimize background from non-specifically adsorbed dye molecules during single-molecule experiments, glass coverslips were coated with a poly-L-lysine-graft-(polyethylene glycol) copolymer functionalized with RGD, as previously described[75]. The assay was performed twice, and a representative blot is presented. Localization and quantification of individual IFNα2 M148A molecules were determined by using the multiple target tracking algorithm (MTT)[76], as previously described[22].

IFN FITC labeling and binding affinity assay. Recombinant IFNα2b (ProSpec, CYT-205) was labeled with fluorescein isothiocyanate (FITC) with a SureLINK FITC-Labeling Kit (KPL, 82-00-01), per the manufacturer's instructions. A conjugate with an optimal molar ratio (F/P) of ~4.1 was used for binding affinity experiments. For binding affinity experiments, the indicated cell lines were incubated with a saturating concentration of FITC-IFNα2b, and FITC MFI was measured on a BD FACSCanto instrument with standard lasers and optical filters.

Receptor expression analysis. Infected U6A cell lines were trypsinized and incubated with mouse anti-IFNAR1 (ref. 77) or IFNAR2-FITC antibodies (Sino Biological, 10359-H08H). For the detection of IFNAR1, we used anti-mouse PE secondary antibody (Invitrogen A10543). Validation of commercial antibodies is available on the manufacturers' websites.

Peptides. THP-1 or KT-1 cells were treated with 10 mM TAT (GRKKRRQRRRPQ) or USP18 aa 302–313–linker (YELFAVIAHVGMGGGS)–TAT (Eton Bioscience) in 2% FBS medium.

Apoptosis assay. Apoptosis was measured on the basis of staining with annexin V-APC and 7-AAD with an annexin V apoptosis detection kit (BD), according to the manufacturer's protocol. Cells were analyzed through flow cytometry on a BD FACSCanto with standard lasers and optical filters. The results in the paper are the means of the percentages of apoptotic cells from three independently infected (MIP or MIP-STAT2 CC/DB 3A) or peptide (TAT or USP18 aa 302–313 TAT)-treated cells.

Statistical analyses. When applicable, statistical significance was determined with two-tailed Student's *t* tests in statcel2 software (OMS). A P value <0.05 was considered to be statistically significant. Changes in the interactions between different bait and prey proteins in the single-molecule ligand binding assay and cell micropatterning experiments, as determined by the contrast values, were statistically analyzed with two-sample Kolmogorov–Smirnov tests. The P values for the contrast values of two samples were calculated in MATLAB software. A P value <0.05 was considered to be statistically significant.

Data availability. Source data for all immunoblots in this study are available in **Supplementary Data Set 1**. Other data supporting our findings in the study are available from corresponding authors upon reasonable request.

61. Colland, F. *et al.* Functional proteomics mapping of a human signaling pathway. *Genome Res.* **14**, 1324–1332 (2004).
62. James, P., Halladay, J. & Craig, E.A. Genomic libraries and a host strain designed for highly efficient two-hybrid selection in yeast. *Genetics* **144**, 1425–1436 (1996).
63. Urbé, S. *et al.* Systematic survey of deubiquitinase localization identifies USP21 as a regulator of centrosome- and microtubule-associated functions. *Mol. Biol. Cell* **23**, 1095–1103 (2012).
64. Roder, F., Birkholz, O., Beutel, O., Paterok, D. & Piehler, J. Spatial organization of lipid phases in micropatterned polymer-supported membranes. *J. Am. Chem. Soc.* **135**, 1189–1192 (2013).
65. Subach, O.M. *et al.* Conversion of red fluorescent protein into a bright blue probe. *Chem. Biol.* **15**, 1116–1124 (2008).
66. Ritchie, K.J. *et al.* Dysregulation of protein modification by ISG15 results in brain cell injury. *Genes Dev.* **16**, 2207–2212 (2002).
67. Boussif, O. *et al.* A versatile vector for gene and oligonucleotide transfer into cells in culture and *in vivo*: polyethylenimine. *Proc. Natl. Acad. Sci. USA* **92**, 7297–7301 (1995).
68. Waichman, S. *et al.* Functional immobilization and patterning of proteins by an enzymatic transfer reaction. *Anal. Chem.* **82**, 1478–1485 (2010).
69. Wedeking, T. *et al.* Spatiotemporally controlled reorganization of signaling complexes in the plasma membrane of living cells. *Small* **11**, 5912–5918 (2015).
70. Arimoto, K. *et al.* Plakophilin-2 promotes tumor development by enhancing ligand-dependent and -independent epidermal growth factor receptor dimerization and activation. *Mol. Cell. Biol.* **34**, 3843–3854 (2014).
71. Muster, B. *et al.* Respiratory chain complexes in dynamic mitochondria display a patchy distribution in life cells. *PLoS One* **5**, e11910 (2010).
72. Sprague, B.L., Pego, R.L., Stavreva, D.A. & McNally, J.G. Analysis of binding reactions by fluorescence recovery after photobleaching. *Biophys. J.* **86**, 3473–3495 (2004).
73. Sprague, B.L. & McNally, J.G. FRAP analysis of binding: proper and fitting. *Trends Cell Biol.* **15**, 84–91 (2005).
74. Vogelsang, J. *et al.* A reducing and oxidizing system minimizes photobleaching and blinking of fluorescent dyes. *Angew. Chem. Int. Edn Engl.* **47**, 5465–5469 (2008).
75. VandeVondele, S., Vörös, J. & Hubbell, J.A. RGD-grafted poly-L-lysine-graft-(polyethylene glycol) copolymers block non-specific protein adsorption while promoting cell adhesion. *Biotechnol. Bioeng.* **82**, 784–790 (2003).
76. Sergé, A., Bertaux, N., Rigneault, H. & Marguet, D. Dynamic multiple-target tracing to probe spatiotemporal cartography of cell membranes. *Nat. Methods* **5**, 687–694 (2008).
77. Goldman, L.A. *et al.* Characterization of antihuman IFNAR-1 monoclonal antibodies: epitope localization and functional analysis. *J Interferon Cytokine Res.* **19**, 15–26 (1999).